Journal of Medicinal Chemistry

Subscriber access provided by UNIV OF CAMBRIDGE

Article

Fragment-Based Drug Discovery Targeting Inhibitor of Apoptosis Proteins: Discovery of a Non-Alanine Lead Series with Dual Activity Against cIAP1 and XIAP

Gianni Chessari, Ildiko M Buck, James Edward Harvey Day, Philip John Day, Aman Iqbal, Christopher Norbert Johnson, Edward Jonathan Lewis, Vanessa Martins, Darcey Lynn Miller, Michael Reader, David Charles Rees, Sharna Jayne Rich, Emiliano Tamanini, Marc Vitorino, George A Ward, Pamela Ann Williams, Glyn Williams, Nicola Elizabeth Wilsher, and Alison J.-A. Woolford

J. Med. Chem., **Just Accepted Manuscript** • DOI: 10.1021/acs.jmedchem.5b00706 • Publication Date (Web): 28 Jul 2015

Downloaded from http://pubs.acs.org on August 1, 2015

Just Accepted

"Just Accepted" manuscripts have been peer-reviewed and accepted for publication. They are posted online prior to technical editing, formatting for publication and author proofing. The American Chemical Society provides "Just Accepted" as a free service to the research community to expedite the dissemination of scientific material as soon as possible after acceptance. "Just Accepted" manuscripts appear in full in PDF format accompanied by an HTML abstract. "Just Accepted" manuscripts have been fully peer reviewed, but should not be considered the official version of record. They are accessible to all readers and citable by the Digital Object Identifier (DOI®). "Just Accepted" is an optional service offered to authors. Therefore, the "Just Accepted" Web site may not include all articles that will be published in the journal. After a manuscript is technically edited and formatted, it will be removed from the "Just Accepted" Web site and published as an ASAP article. Note that technical editing may introduce minor changes to the manuscript text and/or graphics which could affect content, and all legal disclaimers and ethical guidelines that apply to the journal pertain. ACS cannot be held responsible for errors or consequences arising from the use of information contained in these "Just Accepted" manuscripts.

ACS Publications

Journal of Medicinal Chemistry is published by the American Chemical Society. 1155 Sixteenth Street N.W., Washington, DC 20036

Published by American Chemical Society. Copyright © American Chemical Society. However, no copyright claim is made to original U.S. Government works, or works produced by employees of any Commonwealth realm Crown government in the course of their duties.

Fragment-Based Drug Discovery Targeting Inhibitor of Apoptosis Proteins: Discovery of a Non-Alanine Lead Series with Dual Activity Against cIAP1 and XIAP

Gianni Chessari,* Ildiko M. Buck, James E. H. Day, Philip J. Day, Aman Iqbal, Christopher N. Johnson, Edward J. Lewis, Vanessa Martins, Darcey Miller, Michael Reader, David C. Rees, Sharna J. Rich, Emiliano Tamanini, Marc Vitorino, George A. Ward, Pamela A. Williams, Glyn Williams, Nicola E. Wilsher, Alison J.-A. Woolford

Astex Pharmaceuticals, 436 Cambridge Science Park, Milton Road, Cambridge CB4 0QA, U.K.

ABSTRACT

Inhibitor of apoptosis proteins (IAPs) are important regulators of apoptosis and pro-survival signaling pathways, whose deregulation is often associated with tumor genesis and tumor growth. IAPs have been proposed as targets for anticancer therapy and a number of peptidomimetic IAP antagonists have entered clinical trials. Using our fragment-based screening approach, we identified non-peptidic fragments binding with millimolar affinities to both cellular inhibitor of apoptosis protein 1 (cIAP1) and X-linked inhibitor of apoptosis protein (XIAP). Structure-based hit optimization together with an analysis of protein-ligand electrostatic potential complementarity allowed us to significantly increase binding affinity of the starting hits. Subsequent optimization gave a potent non-alanine IAP antagonist structurally distinct from all IAP antagonists previously reported. The lead compound had activity in cell-based assays and in a mouse xenograft efficacy model and represents a highly promising start point for further optimization.

INTRODUCTION

Evasion of apoptosis is one of the hallmarks of cancer[1] and can be achieved by over expression of anti-apoptotic proteins. Inhibitor of apoptosis proteins (IAP), such as cellular IAP1 (cIAP1) and X-linked IAP (XIAP), are key regulators of anti-apoptotic and pro-survival signaling pathways.[2] Their deregulation occurs in various cancers and is associated with tumor growth, poor prognosis and resistance to treatment, making them attractive targets for anti-cancer therapy.[3]

IAPs are characterized by baculovirus IAP repeat (BIR) domains which mediate protein-protein interactions; some members of the family such as cIAP1 and XIAP also possess RING (Really Interesting New Gene) zinc finger domains with E3 ubiquitin ligase activity.[4] XIAP exerts anti-apoptotic activity by binding and inactivation of caspases 3, 7 and 9 via its BIR domains; caspases 3 and 7 bind to the linker between BIR domains 1 and 2, whilst the N-terminal ATPF sequence of caspase 9 is bound in the peptide binding groove of the BIR3 domain.[5] As well as inhibiting apoptosis through the inactivation of caspases, other IAPs (in particular cIAP1 and 2) affect the balance between pro-apoptotic and pro-survival signaling, promoting the formation of complex I[6] in response to TNFα, which activates survival signaling through the canonical NF-κB pathway.[7] Second Mitochondria derived Activator of Caspases (SMAC) is an endogenous IAP antagonist, which is released from mitochondria on induction of apoptosis. SMAC binds to the BIR domains of IAPs and can disrupt interactions between XIAP and caspases.[8] SMAC binding to cIAP1 induces a conformational change which activates its E3 ligase function, leading to rapid autoubiquitinylation and proteasomal degradation.[9] Following removal of cIAP1, RIPK1 recruits FADD and caspase-8 to form complex-IIB, leading to a switch in TNFα signaling from pro-survival to pro-apoptotic.[10] This loss of cIAP1, combined with antagonism of XIAP-mediated caspase inhibition, leads to a sustained pro-apoptotic effect in the presence of TNFα, suggesting that tumors with

sufficient levels of TNFα in their environment may be particularly susceptible to IAP antagonism. It has been suggested that potent and dual cIAP1/XIAP antagonists are more efficient in activating apoptosis than unbalanced cIAP1 antagonists.[11]

The endogenous ligand SMAC binds to the BIR3 domains of cIAP1 and XIAP via its N-terminal peptide sequence AVPI.[8b] This tetrapeptide motif has provided the starting point for various peptidomimetic approaches[12] which have resulted in the discovery of several monovalent and bivalent clinical candidates,[13] some of which are illustrated in Figure 1.

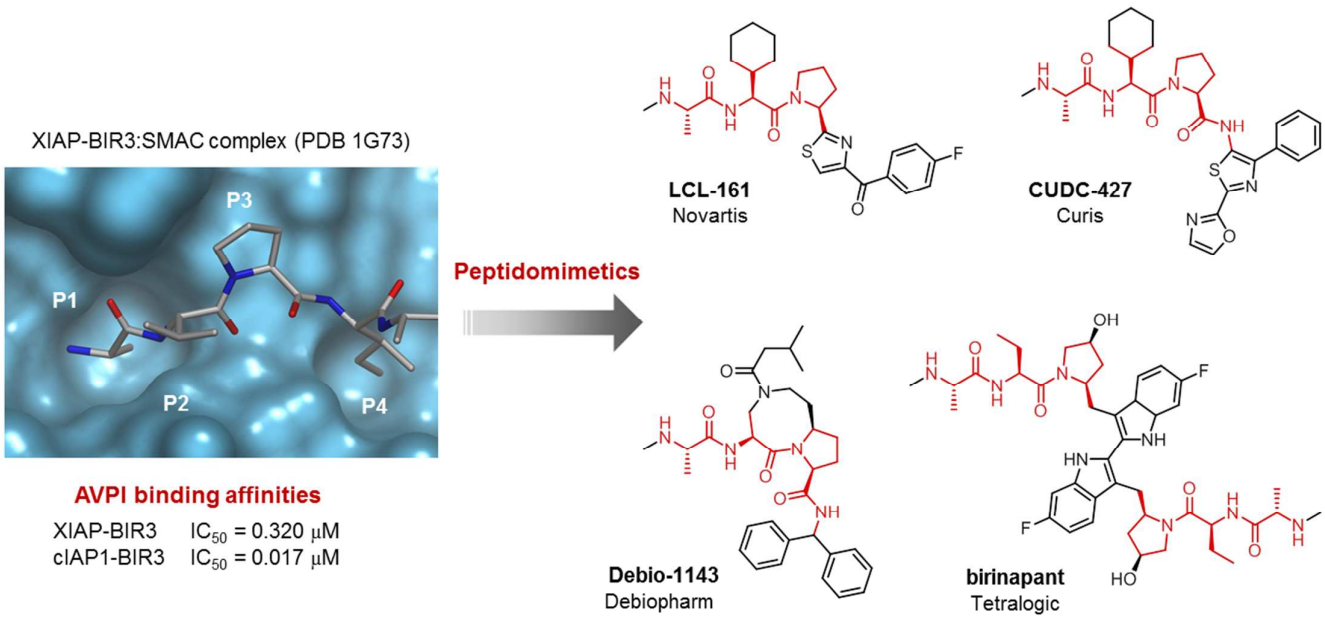

Figure 1. IAP antagonists in clinical trials showing derivation from SMAC N-terminal sequence AVPI.

AVPI itself can bind to the BIR3 domain of cIAP1 or XIAP (cIAP1-BIR3, XIAP-BIR3) occupying subpockets P1-P4 (Figure 1), and shows 18 fold selectivity for cIAP1-BIR3 over XIAP-BIR3. This intrinsic selectivity is mainly due to the differential interactions formed by the alanine residue in the P1 pocket of the BIR3 domains of XIAP and cIAP1 and is usually maintained in alanine-based SMAC mimetic inhibitors.

Fragment-based drug discovery (FBDD) has become both a complementary and an alternative approach to more traditional drug discovery methods (e.g. high-throughput screening, peptidomimetics) for the generation of chemical leads,[14] particularly for challenging and less tractable targets such as Protein-Protein Interaction (PPI) targets.[15] Astex Pharmaceuticals has applied its FBDD technology platform (Pyramid^{TM})[16] to a range of target classes and, in this paper, we describe the use of Pyramid^{TM} to identify new non-alanine hits, with the potential to be developed into potent and balanced XIAP and cIAP1 antagonists.

FRAGMENT SCREENING

The Astex fragment library and a focused fragment set containing 100 fragments selected by virtual screening were screened against XIAP-BIR3. The first step of the screening cascade was based on observing protein signals in 1D NMR experiments. Ligand-detected NMR methods, such as LOGSY or STD-NMR that are commonly used to detect fragment binding, were found to be relatively insensitive for XIAP due to the small size of the protein (11.8 kDa). A protein concentration of 200 μM allowed the use of the protein ^{1}H-NMR spectrum to detect fragment binding by monitoring the chemical shifts and linewidths of XIAP-BIR3 ^{1}H signals with δ <0.4 ppm. NMR signals in this chemical shift range arise from strongly shielded protons in aliphatic side chains. None of the fragment ^{1}H NMR spectra had signals in this region. In addition the range δ 9.8-10.4 ppm was also monitored; in XIAP-BIR3 this region contains four signals, arising from the indole NH protons of tryptophan side chains, two of which are in the binding pocket of interest. Both of these regions of the NMR spectrum contain a number of signals which are strongly affected by the binding of SMAC-derived peptides with sequences AV, AVP and AVPI and so were also expected to be sensitive to fragment binding in the canonical AVPI pocket (data not shown). In total, 1151 fragments were screened against XIAP-BIR3 in cocktails of two. In order to detect very weakly-binding hits, each fragment was present at a concentration of 10 mM. We believe that

under these conditions it was possible to detect ligands binding to XIAP-BIR3 with dissociation constant (K_d) of 30 mM or better.

Figure 2 shows representative XIAP-BIR3 ^{1}H NMR spectra obtained during fragment screening. Figure 2A shows overlaid spectra (δ 0.4-0.3 ppm) from cocktails which contain no fragment hits. In contrast Figure 2B shows the same spectral region from samples containing hits. A number of signals shift and gain intensity as fragments bind, presumably as a result of changes in conformation and mobility of amino acid side chains around the AVPI pocket of XIAP-BIR3.

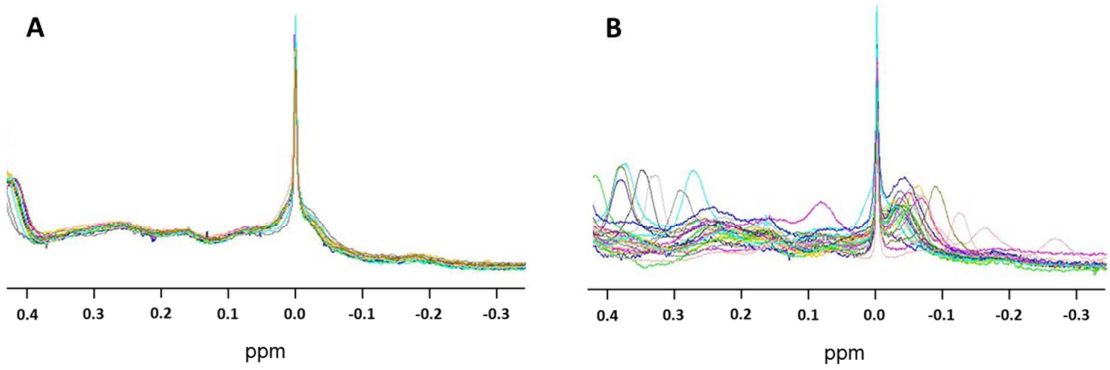

Figure 2. Overlaid ^{1}H NMR spectra of XIAP-BIR3 in the presence of fragment cocktails: (A) containing no hits and (B) containing hits.

Cocktails which contained hits were deconvoluted and fragments responsible for the shift changes were identified and further characterized by a ^{1}H-^{15}N HSQC NMR experiment using ^{15}N labeled XIAP-BIR3 (data not shown).

An X-ray based fragment screen of XIAP-BIR3 was also undertaken using crystals of XIAP-BIR3 (residues 250-354) grown in the absence of compound (for details, see Experimental Section). Fragments were soaked into crystals for 24-72 hours either as singletons (at 50-100

mM fragment, 5-10% DMSO) or doublets (2 x 50 mM, 10% DMSO). In addition, fragment hits, previously identified by NMR screening and/or high concentration bioassay, were soaked into XIAP crystals.

Description of fragment hits

The majority of the fragment hits contained small primary or secondary aliphatic amines, consistent with the known binding site preference for N-terminal alanine-containing peptides. The chemical structures for four fragment hits from the focused fragment set are reported in Table 1, together with IC_{50} values or %I for the BIR3 domains of XIAP and cIAP1. The binding modes were determined by X-ray crystallography.

Table 1. Chemical structures of four hits from fragment screening against XIAP-BIR3 with binding affinity for the BIR3 domains of XIAP and cIAP1.

Compound	Structure	XIAP-BIR3[a] IC_{50} (μM) or %I	XIAP-BIR3 LE[b] (kcal mol^{-1} per non-H atom)	cIAP1-BIR3[a] IC_{50} (μM) or %I
1	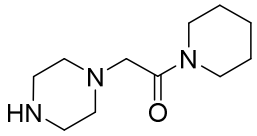	38% at 5 mM	<0.21	16% at 5 mM
2	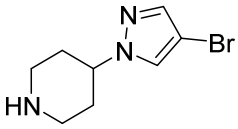	33% at 5 mM	<0.26	55% at 5 mM
3	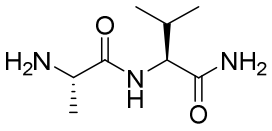	1200	0.30	24
4	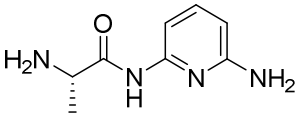	110	0.42	27

[a] Values were determined by fluorescence polarization assay (see Experimental Section). Potency data are reported as the mean of at least two runs. [b] Values calculated according to the Hopkins formula.[17]

Compounds **1** and **2** are weakly binding fragments with affinities above 5 mM for both XIAP-BIR3 and cIAP1-BIR3. Their detection was only possible because of the high sensitivity of X-ray crystallography and NMR techniques used in the fragment screening. Ligand efficiencies (LEs)[17] are low and inferior to the LE values observed for the alanine based fragments **3** and **4**. The binding mode for compound **1** in the BIR3 domain of XIAP is shown in Figure 3A. The piperazine ring lies in the P1 pocket with the protonated nitrogen forming a bidentate hydrogen bond interaction with the Glu314 side chain and the backbone carbonyl of Asp309. The carbonyl of the central amide forms a hydrogen bond with the backbone NH of Thr308 and, in addition, the piperidine ring stacks against the side chain of Trp323 in the P3 pocket. Piperazine containing molecules have been independently identified in a biophysical screen of a XIAP-BIR3 G306E mutant,[18] but subsequent optimization was not described.

The piperidine ring of compound **2** also forms a bidendate hydrogen bond interaction in the P1 pocket of XIAP-BIR3 similar to that observed for compound **1** (see Figure 3B). The bromo-pyrazole is in van der Waals contact with the side chain of Leu307 and forms an edge-to-face aromatic interaction with Trp323, while the non-substituted pyrazole nitrogen forms a hydrogen bond with the backbone NH of Thr308.

Fragment **3** is an alanine-valine dipeptide, which binds to the P1 and P2 pockets of XIAP-BIR3 (Figure 3C). The positively charged primary amine of the alanine forms a charge-charge interaction with the carboxylic group in the side chain of Glu314 and an additional hydrogen bond with the side chain of Gln319. The methyl group of the alanine inserts into the small P1 hydrophobic pocket where it stacks on top of Trp310. The valine forms two β-sheet-like hydrogen bonds with Thr308. The binding mode of **3** is consistent with X-ray crystal structure of the N-terminal sequence of SMAC bound to XIAP-BIR3.[8b]

Compound **4** is another example of an alanine-like fragment identified from the screen, where the alanine recognition is similar to that observed for fragment **3**. The pyridine ring stacks on the top of Leu307 and forms an edge-to-face aromatic interaction with the side chain of Trp323, whilst the pyridine nitrogen is hydrogen bonded to the backbone NH of Thr308. Heterocycles properly functionalized with an alanine warhead similar to compound **4** have previously been reported to bind to XIAP-BIR3 with similar affinity to the natural AVPI peptide.[19]

All alanine based hits from our screen are characterized by relatively high LE for both XIAP and cIAP1, but these fragments show an unbalanced profile with greater than 10 fold selectivity towards cIAP1. We reasoned that their optimization could lead to compounds with a biological profile similar to peptidomimetics currently in clinical development. Non-alanine fragment hits based on the piperazine or piperidine scaffold are weak binders of both XIAP and cIAP1, with LEs well below the benchmark value of 0.3. However, we were interested to explore their potential as a starting point for a more balanced dual XIAP and cIAP1 antagonist. In this paper we report the optimization of fragment **1** into a lead molecule with *in vivo* antitumor activity.

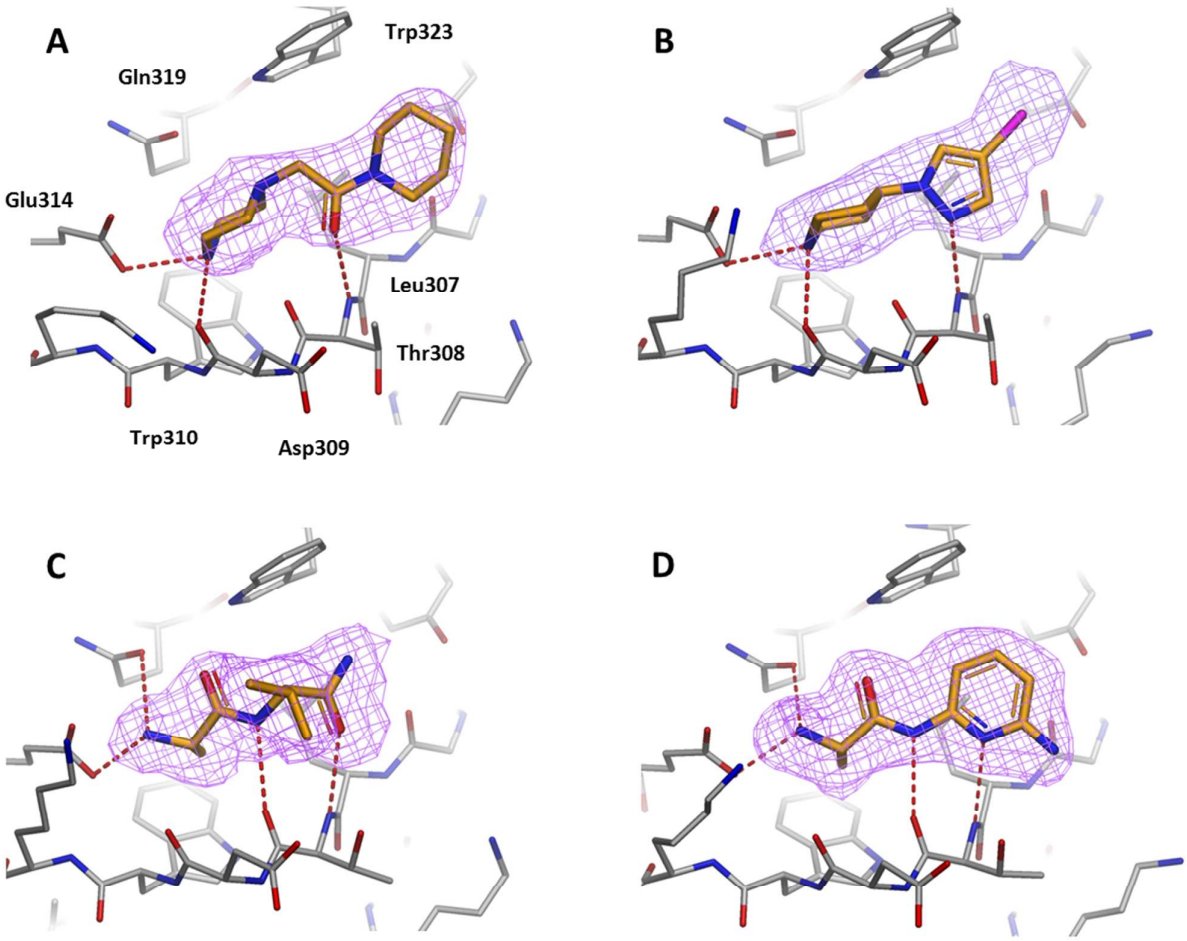

Figure 3. X-ray crystal structures of fragments **1** - **4** bound to XIAP-BIR3 (A to D respectively). The purple mesh represents the initial electron density map (F_o – F_c maps contoured at 1σ and clipped around the ligand) and hydrogen bonds are shown as dashed red lines.

PIPERAZINE FRAGMENT OPTIMIZATION

Comparison of the binding mode of fragment hit **1** with that of alanine fragment hits **3** and **4** provided a good hypothesis for improving affinity. The crystal structure of XIAP-BIR3 with **1** shows that the piperazine does not fill the small lipophilic pocket in P1, where the alanine methyl side chain binds forming a van der Waals contact with the Trp310 side chain. An overlay between fragment **1** and Ala-Val **3** led to the design and synthesis of compound **5**, where the carbon adjacent to the piperazine nitrogen has been substituted by a methyl group,

in order to increase the contacts with the P1 pocket. Compound **5** showed improved potency and LE and its superior filling of the P1 pocket was confirmed by crystallography (see Figure 4).

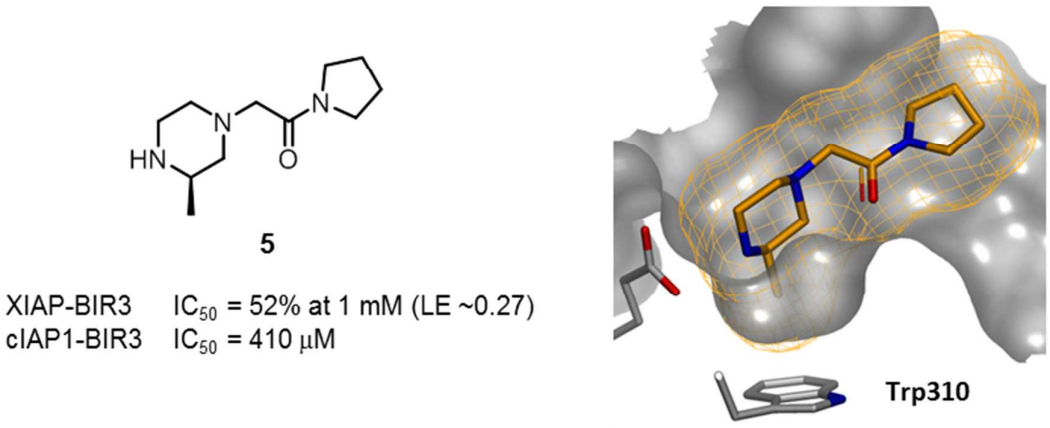

Figure 4. Compound **5** affinity data and binding mode in XIAP-BIR3 as determined by X-ray crystallography showing good shape complementarity in the P1 pocket between the Connolly surfaces of protein (solid gray) and the Connolly surface of the ligand (orange mesh).

The next design iteration investigated a selection of tertiary amides to replace the pyrrolidine in compound **5**. A small virtual library (Heavy Atom Count < 24 and ClogP < 3) was designed, in order to identify side chains which could form good interactions with the P3 pocket and also could provide good vectors to allow entry into the P4 pocket. All the members of the virtual library were docked against XIAP-BIR3. Binding modes were visually inspected and 30 compounds were selected for synthesis. Compounds were prepared by coupling 2-[(3R)-4-[(tert-butoxy)carbonyl]-3-methylpiperazin-1-yl]acetic acid (**6,** R^2 = H, see Figure 5) with a range of aliphatic and aromatic amines, and subsequently removing the Boc protecting group.

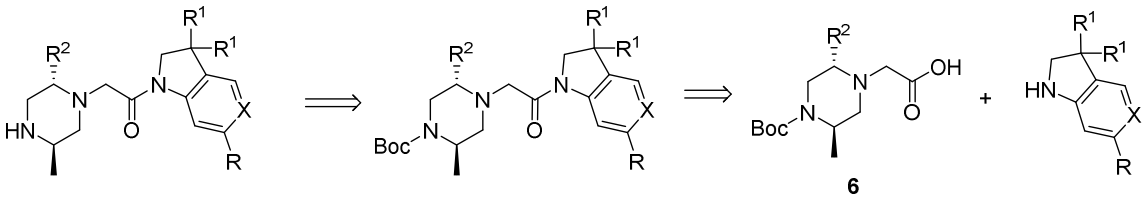

Figure 5. Retrosynthetic analysis for non-alanine IAP antagonists. Protected piperazine-carboxylic acids (see Scheme 1) and bicyclic amines (see Scheme 3) are coupled together before final Boc deprotection.

The resulting compounds were initially evaluated using fluorescence polarization (FP) assays and X-ray crystal structures were attempted by soaking to confirm binding to XIAP-BIR3. Unfortunately, all members of the compound set showed potencies which were comparable or inferior to compound **5**, and improvements in binding affinity and LE were not achieved. However, it was possible to obtain X-ray crystal structures of some members of the set bound to XIAP-BIR3. In particular the structure of indoline **7** (Table 2 and Figure 6) is in good agreement with the design hypothesis; the piperazine warhead forms the same interactions as the optimized fragment **5** and the indoline side chain binds to the P3 region as expected from the modeling.

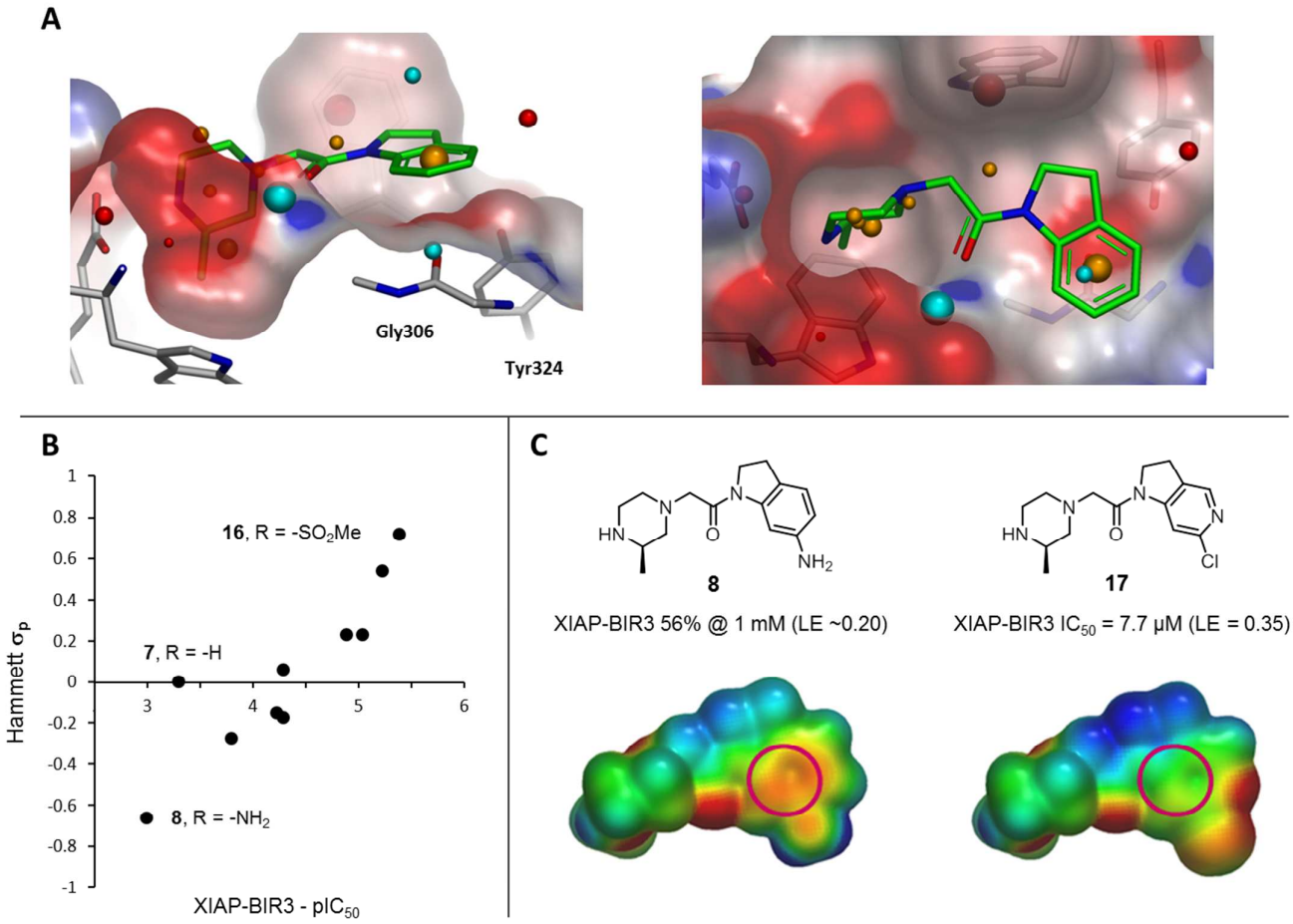

Figure 6. (A) Orthogonal views of compound **7** (green) bound to XIAP-BIR3 as determined by X-ray crystallography. The Connolly surface of the protein is colored by electrostatic potential (red = negative, blue = positive) and ligand Cresset field points as colored spheres (red = positive, blue = negative, orange = lipophilic). (B) Plots of Hammett σ_p coefficients versus XIAP-BIR3 affinities for C-6 substituted indolines **7 - 16**. (C) XIAP-BIR3 affinity data for compounds **8** and **17** with comparison of molecular electrostatic potential surfaces.

We investigated the electrostatic environment of the XIAP-BIR3 binding pocket, in order to explain the lack of improved affinity for compound **7** (XIAP-BIR3 52% at 495 μM, cIAP1-BIR3 42% at 495 μM). The electrostatic potential map obtained for the XIAP-BIR3 binding

site (see Figure 6A) clearly indicated an electronegative patch in the P3 sub-pocket which is due to the presence of the backbone carbonyl of Gly306 and the phenolic oxygen in the side chain of Tyr324. The X-ray crystal structure of compound **7** showed that the aromatic portion of the indoline ring stacks on the top of the negative patch. In order to understand this interaction, the molecular electrostatic potential of **7** was calculated with the XED force-field,[20] which uses off-atom charges for better representation of electron anisotropy around the ligand. Subsequently, negative and positive electrostatic field points were derived using Cresset technology.[21] Figure 6A shows that the π-cloud of the indoline ring (represented by negative field points above and below the aromatic ring) stacks on the top of the negative patch on the protein surface, generating a potential electrostatic repulsion between ligand and protein, which could explain the low affinity of compound **7**.

In order to test this hypothesis, the electronegativity of the indoline π-clouds was modulated by functionalizing the indoline C-6 with a range of electron-withdrawing and electron-donating substituents (Figure 5; $R^1 = R^2 = H$, X = CH). Hammett σ_p values were used to guide the selection of the substituents.[22] The resulting SAR is summarized in Table 2 and Figure 6B.

Table 2. XIAP-BIR3 affinity of substituted indolines **7 - 16**

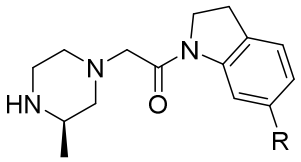

Compound	R	Hammett σ_p	XIAP-BIR3[a] IC_{50} (μM) or %I	XIAP-BIR3 LE[b] (kcal mol^{-1} per non-H atom)
7 (23050)	-H	0.00	52% @ 495 μM	~0.24
8 (23307)	$-NH_2$	-0.66	56% @ 1000 μM	~0.20
9 (23305)	-OMe	-0.27	49% @ 155 μM	~0.25
10 (23306)	-Me	-0.17	46	0.30
11 (23352)	-iPr	-0.15	59	0.26
12 (23330)	-F	0.06	51	0.29
13 (23304)	-Cl	0.23	13	0.33
14 (23132)	-Br	0.23	9.8	0.34
15 (23488)	$-CF_3$	0.54	5.9	0.31
16 (23561)	$-SO_2Me$	0.72	4.1	0.32

[a] See footnote to Table 1

XIAP-BIR3 binding affinities are highly sensitive to the electronic properties of the indoline π-system, with electron-poor indolines (e.g. **15** and **16**) being two orders of magnitude more potent than electron-rich indolines (e.g. **8** and **9**). This dependency is also shown in Figure 6B where binding affinities correlate well with relative Hammett substituent constants σ_p. Interestingly, the unsubstituted indoline **7** appears to be an outlier. This discrepancy could be explained by the van der Waals contribution to binding of the different substituents which is absent for the unsubstituted indoline **7**.

Electrostatic potential surfaces generated with *ab initio* methods also suggested that it was possible to further discharge the π-cloud of the indoline by introducing a nitrogen into the aromatic ring (see Figure 6C). Based on this observation compound **17** was synthesized bearing a chloro substituent suitable for further elaboration to access the P4 pocket. Whilst the binding modes of **17** and **7** are very similar (Figure 7B), careful optimization of the electrostatic interaction between ligand and protein has enabled a >50 fold jump in potency both for XIAP-BIR3 (IC_{50} = 7.7 μM, LE = 0.35) and cIAP1-BIR3 (IC_{50} = 20 μM, LE 0.32) without dramatically changing the size of the ligand. The aza-indoline scaffold also has a positive impact on the lipophilicity of ligand **17**, which has a ClogP of 1.1 and a LLE_{Astex} value[23] of 0.35 (based on XIAP-BIR3 IC_{50}). Importantly, **17** had a balanced XIAP/cIAP1 antagonist profile, vindicating the original decision to pursue a non-alanine fragment hit. The balanced profile of the piperazines can be rationalized by the fact the piperazine warhead forms two similar polar interactions in the P1 pockets of both XIAP-BIR3 and cIAP1-BIR3: a salt bridge to Glu314 for XIAP-BIR3 or Asp314 for cIAP1-BIR3 and an H-bond interaction with the backbone carbonyl of Asp309 for XIAP-BIR3 or Cys309 for cIAP1-BIR3 (see Figure 7). In contrast, the recognition of the alanine warhead (as shown for fragment **3** in the P1 pocket of cIAP1-BIR3) is driven by two charge-charge interactions to Asp309 and Glu319, while in the P1 pocket of XIAP-BIR3 only a single charge-charge interaction is possible, namely to Glu319.

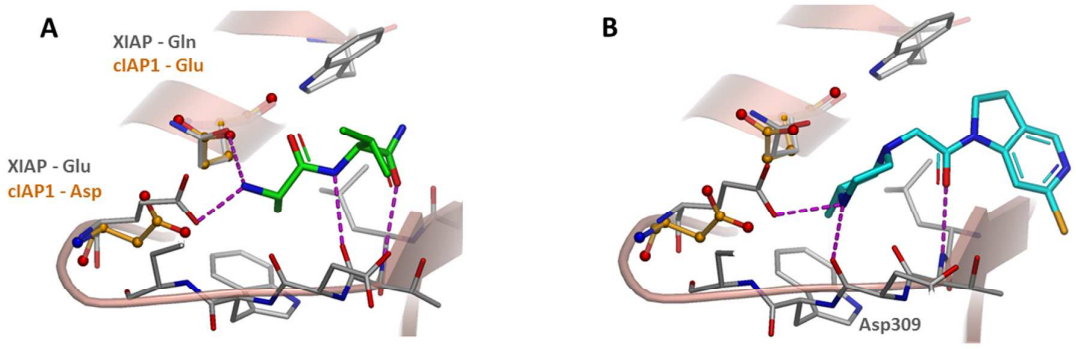

Figure 7. Comparison of binding modes of alanine **3** and piperazine **17** in XIAP-BIR3 (A and B respectively) as determined by X-ray crystallography. Key residue changes for cIAP1 vs. XIAP are shown in orange and hydrogen bonds are shown as purple dashed lines.

The interaction between the indoline side chain and the P3 pockets of XIAP-BIR3 and cIAP1-BIR3 was further optimized by introducing two methyl groups at C-3 of the bicycle, with the aim of increasing the van der Waals contact with Trp323. This change was also introduced to discharge the risk of metabolic oxidation of the indoline to the indole. Indoline **18** showed modestly improved potency compared to the non-methylated analog **13** (see Table 3) and its binding mode in XIAP-BIR3 was consistent with the other indolines (Figure 8A-B). The overlay between the XIAP-BIR3 structure of compound **18** and the tetrapeptide AVPF (see Figure 8A) shows that both P2 and P4 pockets could be targeted by functionalizing C-2 of the piperazine and C-6 of the indoline scaffold respectively. These design ideas were tested by preparing compounds **19**, **20** and **21** (see Table 3).

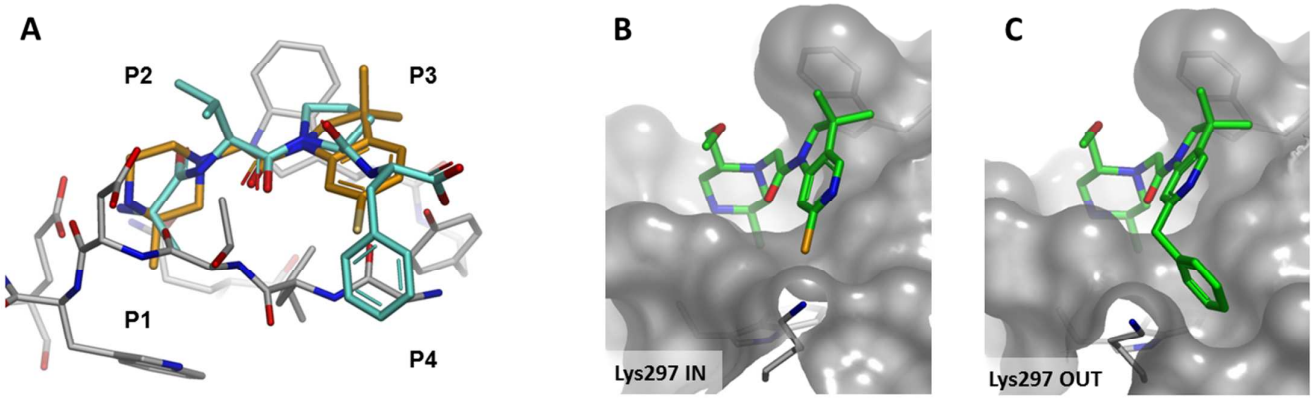

Figure 8. (A) Overlay of X-ray crystal structures of compound **18** (orange) and AVPF (cyan) bound to XIAP-BIR3. (B) and (C) Comparison of X-ray crystal structures of compounds **20** and **21** respectively, showing the effect of Lys297 side chain orientation on the size of the P4 pocket.

Table 3. XIAP-BIR3 and cIAP1-BIR3 binding affinity data for compounds **18-21**.

Compound	Structure	XIAP-BIR3[a] IC_{50} (μM)	XIAP-BIR3 LE (kcal mol^{-1} per non-H atom)	cIAP1-BIR3[a] IC_{50} (μM)
18	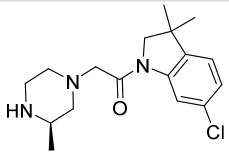	5.5	0.33	3.7
19	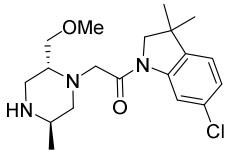	1.5	0.32	0.65
20	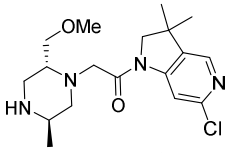	0.64	0.34	0.32
21	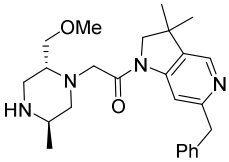	0.16	0.30	0.01
Debio-1143	See Figure 1	70% at 0.05 μM	>0.24	98% at 0.01 μM

[a] see footnote to Table 1.

In compounds **19** and **20** the methoxymethyl side chain was introduced trans at the piperazine C-2 and a jump in potency was observed, with compound **20** being the first compound with sub-micromolar potency for both IAPs. The X-ray crystal structure of compound **20** confirmed the expected binding mode where, interestingly, the P4 pocket is not available because it is occupied by the side chain of Lys297 (see Figure 8B). In compound **21**, C-6 was elaborated with a large side chain in order to target the P4 pocket. The XIAP-BIR3 structure of **21** shows that the side chain of Lys297 moves allowing the benzyl group to bind to the P4 pocket (see Figure 8C). The movement of the Lys297 was anticipated from the crystal structures of SMAC mimetics. This extra lipophilic interaction further improved the potency

of the series and, gratifyingly, compound **21** achieves nM activity for both IAPs. The gain in cIAP1 potency is more pronounced as a result of adding a large lipophilic P4 group suggesting that further optimization of the P4 side chain is required to develop potent and balanced cIAP1 and XIAP antagonists. The contributions to XIAP binding affinity expressed in terms of group efficiency (GE)[24] of the various side chains are summarized in Figure 9.

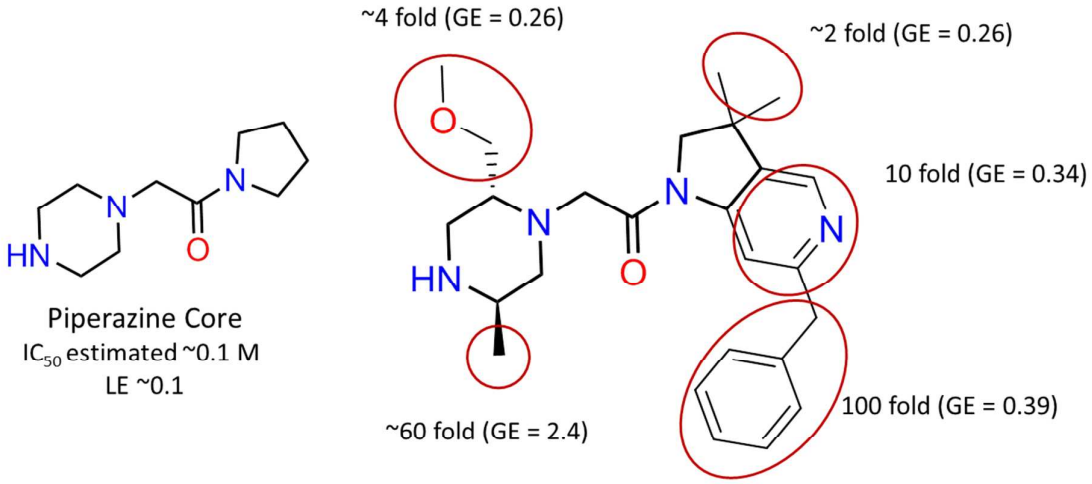

Figure 9. Group efficiency (GE) schematic for compound **21** based on multiple pair-wise comparisons and estimated affinity data for the piperazine core scaffold *vs* XIAP-BIR3. GE units in kcal mol^{-1} per non-H atom.

Compound **21** was tested in cell proliferation assays using two sensitive human breast cancer cell lines (EVSA-T and MDA-MB-231), with the insensitive human colon cancer cell line HCT116 included as a control for off-target cytotoxicity. The clinical compound, Debio-1143 (Debiopharm Group), was included as an assay standard (see Table 4).[13c] EVSA-T and MDA-MB-231 cell lines undergo apoptosis with an IAP antagonist which is driven by autocrine production of TNFα, whilst HCT116 cells are resistant to IAP antagonists due to reduced TNFα production.

The EVSA-T and MDA-MB-231 cell lines are particularly sensitive to cIAP1 antagonism and we desired a direct measure of XIAP antagonism in cells. Hence, we stably transfected HEK293 cells with full-length XIAP (FLAG-tagged) and caspase-9 to generate an engineered cell line in which an immunoprecipitation assay could be used to measure levels of XIAP:Caspase-9 interaction after a 2 h incubation with IAP antagonist. In this assay, **21** was shown to antagonize XIAP with an EC_{50} of 140 nM whilst the anti-proliferative EC_{50} on the cIAP1-sensitive cell line, EVSA-T, was 100 nM (see Table 4). In separate cell-based assays a reduction in cIAP1 levels was measured in EVSA-T cells after 2 h incubation with **21**; and a significant increase in cleaved caspase-3 was induced in EVSA-T cells after 6 h incubation with **21** (data not shown).

Table 4. Compound **21** and Debio-1143 cell-based assay data

Cell Line	Cell-based assay	**21** EC_{50} (μM) (n)	**Debio-1143** EC_{50} (μM) (n)
EVSA-T	Proliferation (72 h)	0.10 (2)	0.0021 (51)
MDA-MB-231	Proliferation (72 h)	0.59 (2)	0.019 (51)
HCT116	Proliferation (72 h)	>10 (2)	>10 (50)
HEK293-XIAP-Caspase-9[a]	Immunoprecipitation (2 h)	0.14 (3)	0.034 (92)

[a] HEK293-XIAP-Caspase-9 is a stably transfected HEK293 cell line engineered to overexpress full-length XIAP (FLAG-tagged) and caspase-9. For further details of all cell-based assays, see Supporting Information.

In order to demonstrate target engagement *in vivo*, a single 100 mg/kg dose of **21** was administered intraperitoneally (i.p.) in Balb/c scid mice bearing MDA-MB-231 xenografts. At 1, 6 and 24 h post dose tumors were harvested for Western blot analysis of xenograft lysates (see Figure 10A). A significant reduction in cIAP1 levels relative to the vehicle-dosed

animal tumors was evident in tumors taken from mice 1 h post dose with compound **21** (this was confirmed by densitometry of the blot and subsequent cIAP1 assay tumor lysates using an Meso-Scale Discovery (MSD) plate-based method for detection of cIAP1 levels – data not shown). However, it was noted that cIAP1 levels were variable at 6 h and had returned to vehicle levels by 24 h, suggesting that plasma and tumor free concentrations were insufficient to produce a prolonged pharmacodynamic effect. Additionally, there was no obvious effect on XIAP levels (indicating that binding of compound **21** to XIAP-BIR3 does not lead to ubiquitin-mediated degradation of XIAP) and only a slight increase in apoptosis markers (cleaved PARP and cleaved caspase-3) in the compound **21** treated animals (see Figure 10A).

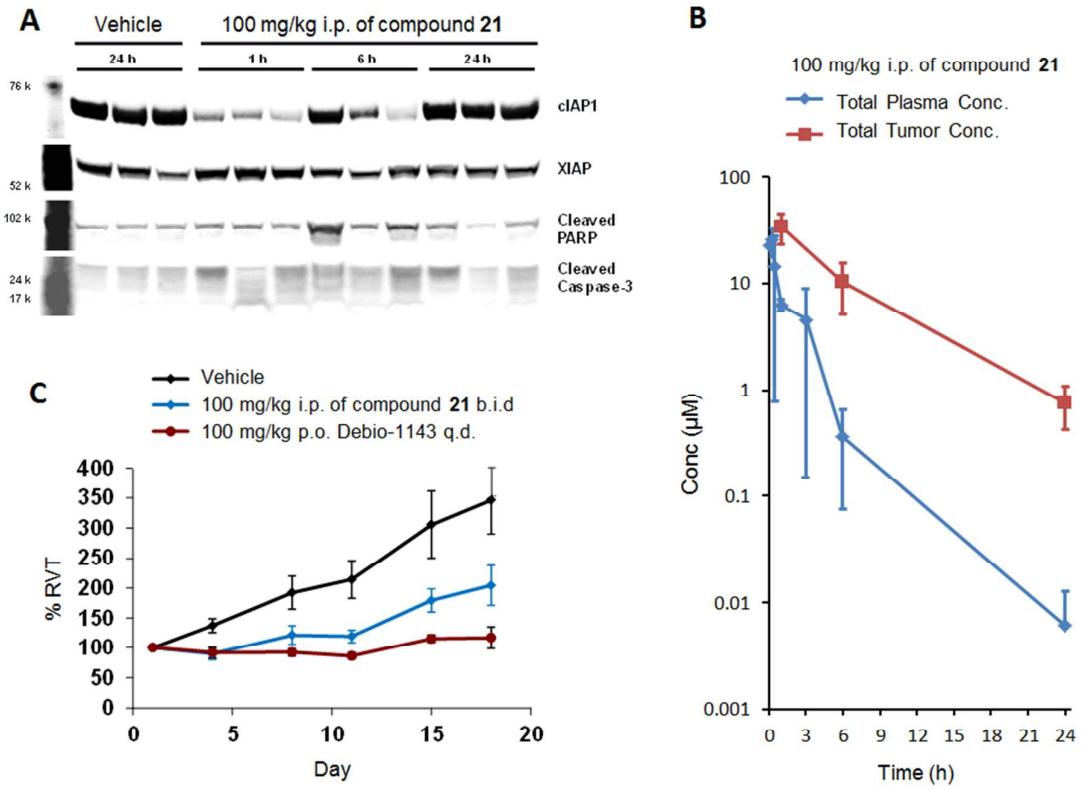

Figure 10. (A) Pharmacodynamic (PD) and (B) Pharmacokinetic (PK) effect of a single 100 mg/kg dose of **21** i.p. in Balb/c scid mice bearing MDA-MB-231 xenografts. (C) *In vivo*

efficacy in Balb/c scid mice bearing MDA-MB-231 xenografts dosed i.p. with **21** at 100 mg/kg b.i.d.

In order to demonstrate efficacy in a mouse xenograft model, 100 mg/kg i.p. doses of **21** were administered b.i.d. in Balb/c scid mice bearing MDA-MB-231 xenografts. As a positive control in this study the clinical IAP antagonist, Debio-1143, was dosed daily (q.d.) at 100 mg/kg p.o. Significant reduction in tumor size was measured with twice daily (b.i.d.) dosing i.p. of **21** (see Figure 10C), with no significant effect on body weight.

CHEMISTRY

The majority of compounds described in this paper were assembled via a convergent synthesis involving late stage amide coupling, as shown in Figure 5, allowing maximum flexibility to explore the SAR in different regions of the protein (see Supporting Information for detailed experimental procedures). The carboxylic acid-functionalized piperazines **22** and **23** were prepared according to Scheme 1 and indolines and azaindolines **24** – **31** according to Scheme 2.

Piperazine **22** was readily prepared from commercially available (R)-2-methyl-piperazine-1-carboxylic acid *tert*-butyl ester by alkylation with benzyl bromoacetate followed by hydrogenolysis of the benzyl group as shown in Scheme 1. The two stereocenters in piperazine **23** are derived from D-alanine methyl ester and Cbz protected L-serine. EDC mediated coupling gave a dipeptide which cyclized *in situ* following hydrogenolysis of the Cbz protecting group. The resulting diketopiperazine was reduced with borane and the product treated with di-tert-butyl dicarbonate. The initially formed bis-Boc derivative was then treated with aqueous ethanolic sodium hydroxide, resulting in selective removal of the Boc group adjacent to the hydroxymethyl substituent, the reaction proceeding via formation

of the bicyclic oxazolidinone. Treatment with benzyl chloroformate then gave the orthogonally protected 2,5-disubstituted piperazine. Alkylation of the hydroxyl group was accomplished using trimethyloxonium tetrafluoroborate in the presence of Proton-Sponge® (1,8-bis(dimethylamino)naphthalene). Following removal of the Cbz group, elaboration to carboxylic acid **23** was performed in a manner similar to that described for **22**.

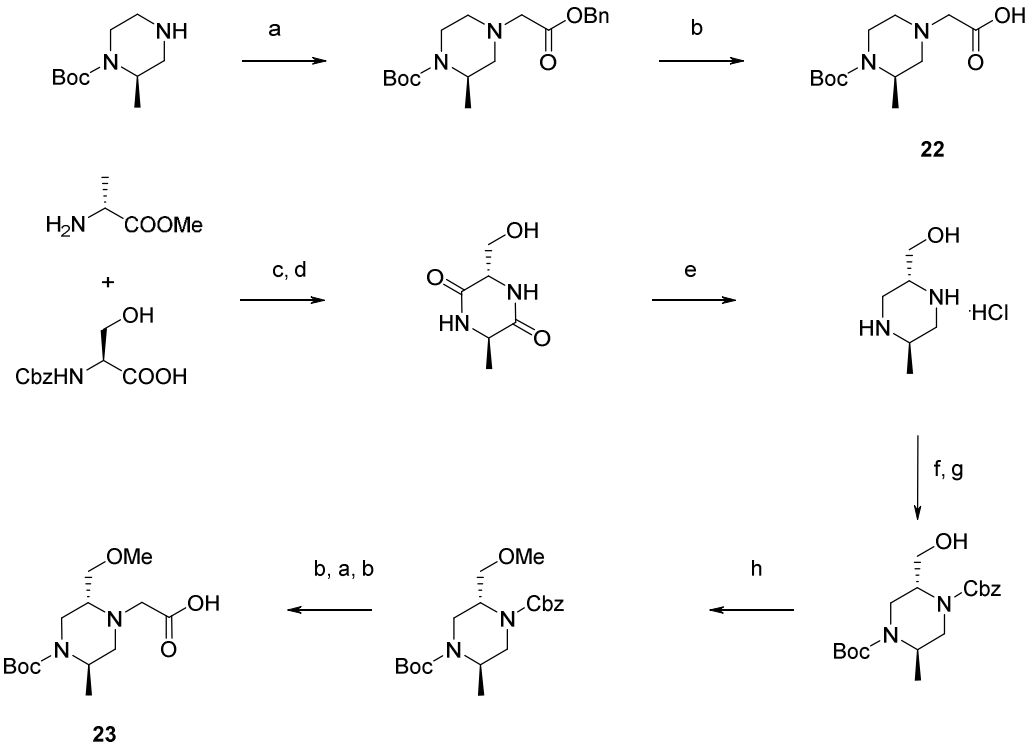

Scheme 1. Reagents and conditions: a) benzyl bromoacetate, K_2CO_3, ACN, R.T., 82%; b) Pd/C, MeOH, H_2, R.T., >94%; c) EDC, DIPEA, DCM, R.T., 74%; d) Pd/C, MeOH, cyclohexene, reflux, 81%; e) BH_3·THF, THF, 70 °C, quant.; f) Boc_2O, TEA, MeOH 50 °C, then NaOH, aq. EtOH, 100 °C, 75%; g) benzyl chloroformate, NaOHaq., THF, R.T., 76%; h) Proton-sponge®, trimethyloxonium tetrafluoroborate, DCM, 5-17 °C, 65%.

The required 6-substituted indolines were either commercially available or could be prepared by reduction of the commercially available indole or aza-indole precursors, using either

borane or $NaBH_3CN$ (Scheme 2, compounds **24** – **29**). The 3,3-dimethyl substituted chloroindoline **30** was synthesized by a modified Fischer indole procedure starting from 3-chlorophenylhydrazine and isobutyraldehyde, in which the desired 6-chloro regioisomer was separated from the 4-chloro by chromatography. The synthesis of the more elaborated 3,3-dimethyl-5-aza-6-chloroindoline **31** is accomplished using a 6 step procedure, starting from commercially available 6-chloro-5-azaindole, introduction of the gem-dimethyl groups being effected by deprotonation of an aza-oxindole intermediate and subsequent treatment with iodomethane.

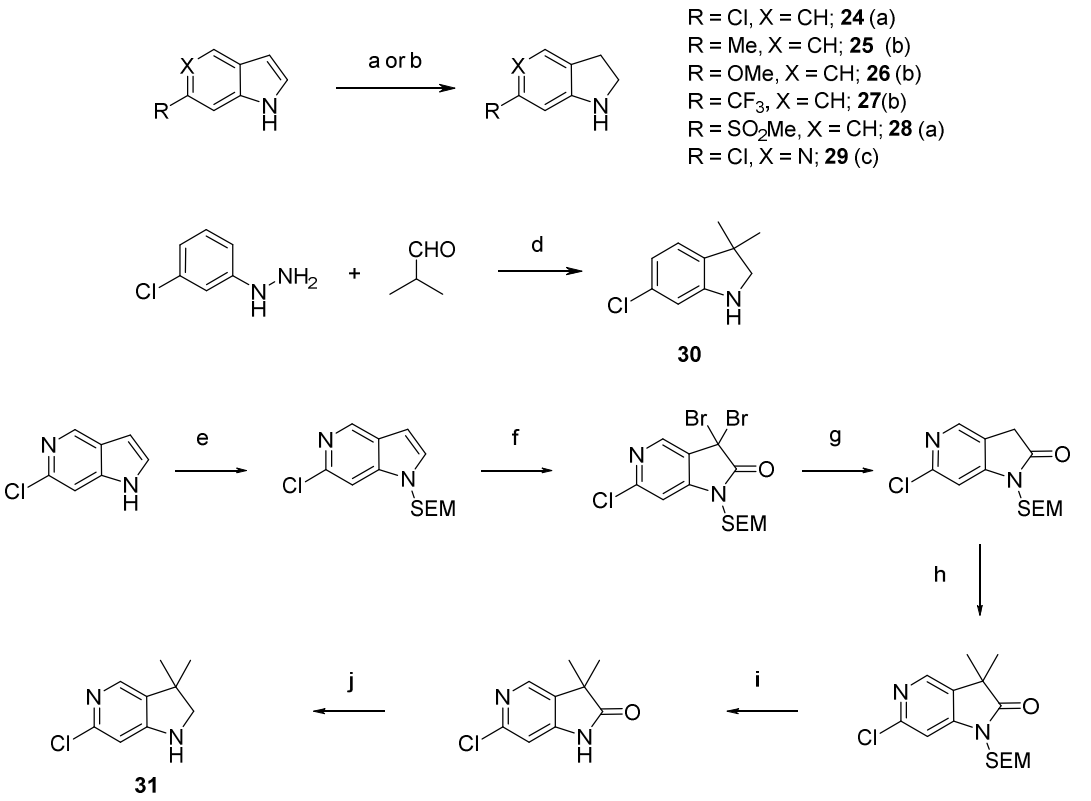

Scheme 2. Reagents and conditions: a) BH_3, THF then TFA, 0 °C, 64-86%; b) $NaBH_3CN$, AcOH, R.T., 35-66%; c) $BH_3.SMe_2$, THF then MeOH, 68 °C, 41%; d) AcOH, 60 °C then $NaBH(OAc)_3$, DCE, R.T., 4%; e) NaH, $(CH_3)_3SiCH_2CH_2OCH_2Cl$, DMF, 0 ºC, 82%; f) $C_5H_5N{\cdot}HBr{\cdot}Br_2$, dioxane, R.T., 58%; g) Zn, NH_4Cl (aq), THF, R.T., 75%; h) LiHMDS, CH_3I, THF, -78 ºC, 51%; i) TFA, DCM, R.T., 67%; j) BH_3-Me_2S, THF, 68 ºC, 95%.

Following the schematic in Figure 5, the appropriate amine and acid precursors were coupled using PyBroP and the products deprotected with concentrated HCl in dioxane as illustrated for compounds **19** and **20** (Scheme 3), to give target compounds **7**, **9**, **10** and **12** - **20**. Optimized fragment **5** was also prepared following similar methods using pyrrolidine in the amide coupling step. Compound **21** was prepared by late stage Negishi coupling of the protected chloro-azaindoline with benzylzinc bromide followed by Boc deprotection.

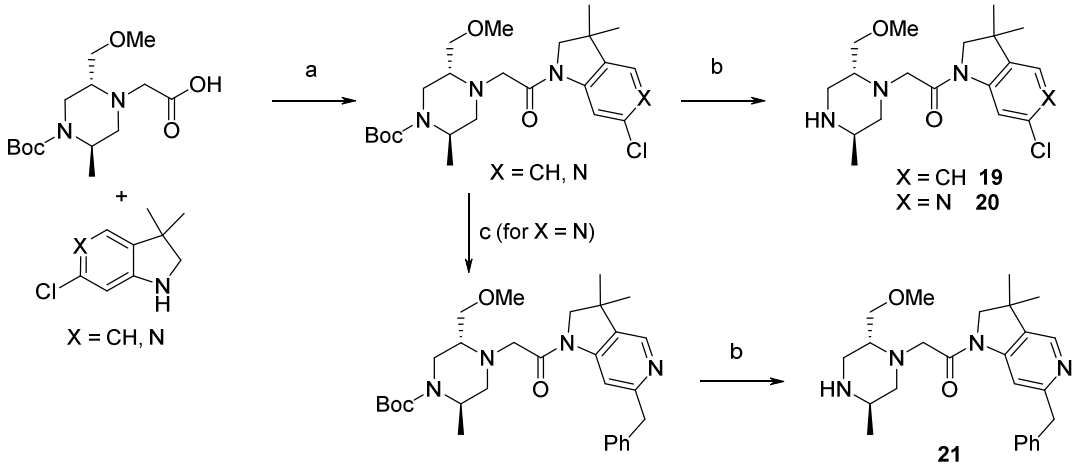

Scheme 3. Reagents and conditions: a) PyBroP, TEA, DCM, R.T., 74%; b) conc. HCl, dioxane, R.T., 78-85%; c) Benzylzinc bromide, PEPPSI^{TM}-IPr, LiBr, NMP, THF, R.T., 78%.

Analogs **8** and **11** were also prepared by late stage elaboration of C-6 on the bicycle (Scheme 4). Compound **8** was prepared via reduction of a 6-nitro indoline derivative, while for **11** the isopropyl group was introduced by Suzuki coupling of 2-isopropenyl-4,4,5,5-tetramethyl-1,3,2-dioxaborolane with a 6-bromo indoline derivative followed by hydrogenation.

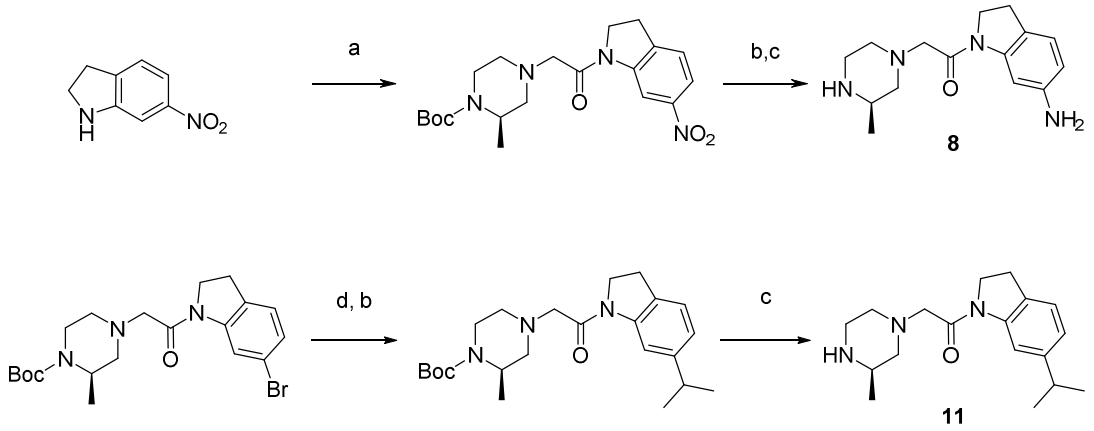

Scheme 4. Reagents and conditions: a) **22**, PyBroP, TEA, DCM, R.T., 50%; b) 10% Pd/C, H_2, MeOH, R.T., quant.; c) conc. HCl, dioxane, R.T., 82%; d) 2-isopropenyl-4,4,5,5-tetramethyl-1,3,2-dioxaborolane, $Pd(PPh_3)_4$, Cs_2CO_3, 85 °C, 86% over 2 steps.

CONCLUSION

We have applied Astex Pyramid™ to XIAP-BIR3 in order to identify non-alanine starting points for antagonists with balanced dual cIAP1/XIAP profiles. A combination of protein observed ^{1}H-NMR screening and X-ray crystallography screening based on long soaking experiments using high fragment concentrations allowed us to identify very weak non-alanine fragment hits. Structure-based drug design coupled to an electrostatic analysis of the XIAP-BIR3 binding site enabled the efficient optimization of the piperazine-based initial hit **1** into a scaffold **17** with low micromolar activity and good LE for both XIAP and cIAP1 BIR3 domains. Subsequent elaboration gave compound **21**, which antagonizes XIAP, induces cIAP1 degradation and inhibits cell growth in cancer cell lines. Biomarker modulation associated with reduction in tumor size was observed in a mouse xenograft model bearing the breast cancer cell line MDA-MB-231 xenografts when treated with 100 mg/kg i.p. doses of **21**. Compound **21** is the first reported example of a nanomolar affinity non peptidic IAP antagonist which does not possess an alanine warhead. Hence **21** represents a novel chemotype for an important class of anticancer targets and has proved a promising starting

point for further medicinal chemistry. Further optimization of **21** into an orally bioavailable and efficacious dual XIAP/cIAP1 antagonist with low nanomolar affinity for both targets will be reported in a subsequent publication.

EXPERIMENTAL SECTION

General Chemistry

All solvents employed were commercially available anhydrous grade, and reagents were used as received unless otherwise noted. Hereafter, petrol denotes the petroleum ether fraction boiling at 40 – 60 ^{o}C. Flash column chromatography was performed on a Biotage SP1 system (32−63 μm particle size, KP-Sil, 60 Å pore size). NMR spectra were recorded on a Bruker AV400 (Avance 400 MHz) spectrometer. Analytical LC−MS was conducted using an Agilent 1200 series with Mass Spec Detector coupled with an Agilent 6140 single quadrupole mass detector and an Agilent 1200 MWD SLUV detector. LC retention times, molecular ion (m/z) and LC purity (by UV) were based on the method below. Purity of compounds (as measured by peak area ratio) was >95%, as determined by the LC method described below.

LC Method (BASIC)

Eluent A: 95:5 10 mM NH_4HCO_3+NH_4OH:CH_3CN (pH = 9.2)

Eluent B: CH_3CN

Gradient: 5-95% eluent B over 1.1 minutes

Flow: 0.9 ml/min

Column: Waters Acquity UPLC BEH C18; 1.7μ; 2.1x50 mm

Column T: 50°C

Preparation of compound 21 (Scheme 3): 1-(6-Benzyl-3,3-dimethyl-2,3-dihydro-pyrrolo[3,2-c]pyridin-1-yl)-2-((2*R*,5*R*)-2-methoxymethyl-5-methyl-piperazin-1-yl)-ethanone hydrochloride salt

Step 1: (2*R*,5*R*)-4-[2-(6-Chloro-3,3-dimethyl-2,3-dihydro-pyrrolo[3,2-c]pyridin-1-yl)-2-oxo-ethyl]-5-methoxymethyl-2-methyl-piperazine-1-carboxylic acid tert-butyl ester

To a solution of (2*R*,5*R*)-4-carboxymethyl-5-methoxymethyl-2-methyl-piperazine-1-carboxylic acid *tert*-butyl ester **23** (4.1 g, 13.7 mmol, see Supporting Information) and 6-chloro-3,3-dimethyl-2,3-dihydro-1H-pyrrolo[3,2-c]pyridine **31** (1.2 g, 6.9 mmol, see Supporting Information) in dichloromethane (34 mL) were added PyBroP (7.7 g, 16.5 mmol) and triethylamine (4.9 mL, 35.7 mmol). The reaction mixture was stirred at ambient temperature for 18 hours. The solvent was removed *in vacuo* and the residue was purified by chromatography on silica gel (gradient elution with 0 – 100% ethyl acetate in petrol) to give the title compound (2.4 g, 73%) as a yellow foam. ^{1}H NMR (400 MHz, $CDCl_3$): 8.09 (1H, s), 8.07 (1H, s), 4.28-4.16 (1H, m), 4.06-3.85 (3H, m), 3.66 (2H, d), 3.56-3.42 (1H, m), 3.42-3.34 (4H, m), 3.31 (1H, dd), 3.03 (1H, s), 2.86 (1H, dd), 2.67 (1H, dd), 1.58 (3H, s), 1.49 (9H, s), 1.42 (6H, s); LCMS: $[M+H]^+ = 467$.

Step 2: (2*R*,5*R*)-4-[2-(6-Benzyl-3,3-dimethyl-2,3-dihydro-pyrrolo[3,2-c]pyridin-1-yl)-2-oxo-ethyl]-5-methoxymethyl-2-methyl-piperazine-1-carboxylic acid tert-butyl ester

(2*R*,5*R*)-4-[2-(6-Chloro-3,3-dimethyl-2,3-dihydro-pyrrolo[3,2-c]pyridin-1-yl)-2-oxo-ethyl]-5-methoxymethyl-2-methyl-piperazine-1-carboxylic acid tert-butyl ester (1.0 g, 2.14 mmol) was added to a solution of PePPSi-iPr (40 mg, 0.06 mmol) and LiBr (390 mg, 4.54 mmol) in NMP (12 mL) and THF (12 mL) under inert atmosphere. The solution was degassed for 5 min before adding benzylzinc bromide (9.1 mL, 1.6 mmol). The reaction was stirred at room temperature for 30 minutes and then quenched with water. The product was extracted with

EtOAc and the organic phase was washed with water and brine. The organic layer was dried over $MgSO_4$, filtered and concentrated in vacuo. The residue was putified by chromatography on silca gel (gradient 0 – 100% EtOAc in Petrol) to give 879 mg (79% yield) of the desired product as a pale yellow oil. ^{1}H NMR (400 MHz, Me-d_3-OD): 8.24 (1H, s), 7.94 (1H, s), 7.34-7.15 (5H, m), 4.85 (2H, s), 4.22-4.07 (3H, m), 4.07-3.87 (3H, m), 3.69 (1H, d), 3.59 (1H, dd), 3.52 (1H, d), 3.42-3.34 (3H, m), 2.99 (1H, s), 2.84 (1H, dd), 2.64 (1H, d), 1.48 (9H, s), 1.42 (6H, s), 1.28-1.10 (3H, m); LCMS: $[M+H]^+ = 523$.

Step 3: 1-(6-Benzyl-3,3-dimethyl-2,3-dihydro-pyrrolo[3,2-c]pyridin-1-yl)-2-((2*R*,5*R*)-2-methoxymethyl-5-methyl-piperazin-1-yl)-ethanone hydrochloride salt **21**

(2*R*,5*R*)-4-[2-(6-Benzyl-3,3-dimethyl-2,3-dihydro-pyrrolo[3,2-c]pyridin-1-yl)-2-oxo-ethyl]-5-methoxymethyl-2-methyl-piperazine-1-carboxylic acid tert-butyl ester (1.57 g, 3.0 mmol) was dissolved in a saturated solution of HCl in EtOAc and the resulting mixture stirred at ambient temperature for 18 hours. The reaction was concentrated *in vacuo* and the residue was azeotroped with MeOH (4 x) to give the title compound (1.27 g, quant.) as an off white solid. ^{1}H NMR (400 MHz, Me-d_3-OD): 8.60 (1H, s), 8.26 (1H, s), 7.48-7.26 (5H, m), 4.58-4.31 (4H, m), 4.31-4.08 (2H, m), 4.08-3.91 (1H, m), 3.90-3.71 (2H, m), 3.71-3.58 (3H, m), 3.58-3.40 (2H, m), 1.54 (6H, s), 1.41 (3H, d); LCMS: $[M+H]^+ = 423$.

Preparation of compounds **5** and **7** through **20** is described in the Supporting Information.

Crystallography

XIAP-BIR3 250-354 was crystallized using a 1:1 ratio of 10 mg/ml protein and 0.1 M Hepes-NaOH pH 8.0, 3.0-3.9 M NaCl. Crystals appeared over the course of a few days at 4 ºC. Crystals were soaked in fragments using 2.5 µl of compound in DMSO, 47.5 µl 0.1 M Hepes-NaOH pH 8.0, 4 M NaCl to give a final concentration of fragment in the range of 50-100 mM. The pH of the soaking solution was adjusted if necessary and crystals were left at 4 ºC

for 24-72 hours. Crystals were cryo-protected using 0.05 M Hepes-NaOH pH 8.0, 4M NaCl, 15% ethylene glycol. The crystals had cell dimensions of approximately 70 Å, 70 Å, 105 Å, and belong to space group P4122. The diffraction observed ranged from 1.7-3.0 Å.

NMR

NMR screening was performed by monitoring the effects of fragments on well-resolved ^{1}H NMR signals of unlabeled XIAP-BIR3 with chemical shifts δ <0.4 ppm and >9.8 ppm. For these experiments 144 μL samples were prepared containing 220 μM XIAP-BIR3, 80 mM sodium phosphate, 20 mM TRIS pH 7.6 and 15% D_2O. A 16μl aliquot of a DMSO stock solution containing two fragments, each at a concentration of 100 mM, was then added to each sample to give a final protein concentration of 200 μM and fragment concentrations of 10 mM, with 10% d_6- DMSO. Previous experiments had shown that this buffer was sufficiently concentrated to maintain the pH of the solution at 7.6 ± 0.2 after fragment addition. Samples were transferred to 2.5 mm (o.d.) capillaries and NMR data collected using a Bruker AV500 spectrometer equipped with a 5 mM TXI-cryoprobe. The sample temperature was maintained at 40 °C during data acquisition and all spectra were acquired with an acquisition time of 8.5 minutes (256 scans). Samples containing hits were broken out to determine the identity of the hit and were then followed up by titration of the hit into a ^{15}N-labeled sample of XIAP-BIR3, and the ^{15}N-HSQC spectrum was monitored for chemical shift changes. Hits could then be prioritized according to their estimated affinity or their chemical shift fingerprint.

Fluorescence Polarization Binding Assay

The interaction between the SMAC peptide and the BIR3 domains of XIAP and cIAP1 was measured using a fluorescence polarization assay, utilizing a fluorescent peptide tracer (AbuRPFK(5&6FAM)-amide; Peptide Synthetics Ltd, Fareham, Hampshire, UK) derived

from SMAC. Compounds were incubated with XIAP (20 nM) or cIAP1 (4 nM) proteins in 50 mM Hepes pH 7.5, 0.025% Tween-20, 0.01% BSA, 1 mM DTT, 2% DMSO and 5 nM or 2 nM fluorescent tracer respectively. After equilibration at room temperature fluorescence polarisation was measured (excitation 485 nm / emission 538 nm) using a BMG Pherastar plate reader (BMG Labtech, Orttenburg, Germany). IC_{50} curves were generated using GraphPad prism version 6 (LaJolla, CA, USA) and fitted using the four parameter logistic curve fit.

Cell Line Proliferation Assay

Inhibition of cell growth was measured using the Alamar Blue assay.[25] For each proliferation assay cells were plated onto 96 well plates and allowed to recover for 16 hours prior to the addition of inhibitor compounds (in 0.1% DMSO v/v) for a further 72 hours. At the end of the incubation period 10% (v/v) Alamar Blue (Bio-Rad AbD Serotec, Oxford, UK) was added and incubated for a further 6 hours prior to determination of fluorescent product at 535 nM excitation / 590 nM emission.

The anti-proliferative activities of **21** or Debio-1143 were determined by measuring the ability of the compounds to inhibit growth in 3 cancer cell lines: (1) EVSA-T (human breast carcinoma) [DSMZ, Braunschweig, Germany], (2) MDA-MB-231 (human breast carcinoma) [ECACC, Salisbury, UK], (3) HCT116 (human colon carcinoma) [ECACC, Salisbury, UK] - insensitive cell line used as a control for non-specific cytoxicity.

XIAP Antagonism Immunoprecipitation Assay

An engineered HEK293 cell line was generated by transfecting the HEK293 cell line (ECACC, Salisbury, UK) with a full-length FLAG-tagged XIAP expression construct [Origene Technologies Inc., Rockville, USA] and a full-length untagged caspase-9 construct

[Origene Technologies, Inc., Rockville, USA]. Stable co-transfectants were selected after culture in selection medium containing Geneticin (Life Technologies, Paisley, UK).

Stable HEK293-XIAP-Caspase-9 cells were plated out into 96-well plates and left overnight at 37 °C to recover. Compounds were added to duplicate wells in 0.1% DMSO for 2 h at 37 °C. Cells were lysed in 50 μL lysis buffer (1% Triton X-100 in 20 mM Tris.Cl (pH 7.6), 150 mM NaCl, including protease inhibitors (Roche Diagnostics Ltd., Burgess Hill, UK) for 20 min rocking at room temperature. Streptavidin-coated high-bind MSD plates (Meso Scale Discovery, Gaithersburg, USA) were coated with biotinylated anti-FLAG M2 antibody (Sigma, Poole, UK) and then blocked with 3% BSA in TBST (20 mM Tris.Cl (pH 7.6), 150 mM NaCl, 0.1% Tween-20). Cell lysate was added to the 96-well anti-FLAG coated MSD plate and placed on a shaker overnight at 4 °C. After washing 3 times with TBST, rabbit anti-Caspase-9 (Cell Signaling Technology Inc., Danvers, USA) was added for 2 h at room temperature, with shaking. After washing 3 times with TBST, anti-rabbit-sulfo tag (Meso Scale Discovery, Gaithersburg, USA was added for 2 hours at RT. Plates were washed 3 times with TBST and then read buffer was added, before reading the plate on a MESO QuickPlex SQ 120 (Meso Scale Discovery, Gaithersburg, USA).

Western Blot Analysis of MDA-MB-231 Xenografts

MDA-MB-231 xenograft tumor lysates were prepared by grinding the frozen tissue to a fine powder with a mortar/pestle under liquid nitrogen, and then adding ice-cold lysis buffer (1% Triton X-100, 150 mM NaCl, 20 mM Tris.HCl pH 7.5, plus protease inhibitors (Roche Diagnostics Ltd., Burgess Hill, UK), 50 mM NaF and 1 mM Na_3V0_4), to the ground-up tumour powder. Samples were vortexed and left on ice for 30 min. Lysates were cleared and sample of the supernatant removed for protein determination (BCA assay – Pierce, Life Technologies, Paisley, UK).

Equivalent amounts of protein lysate had SDS sample buffer and a final concentration of 50 mM DTT added, before being boiled. Samples were resolved by SDS PAGE (4-12% Nu-PAGE gels – Novex, Life Technologies, Paisley, UK), blotted onto nitrocellulose filters, blocked with Odyssey Blocking Buffer (LI-COR, Cambridge, UK) and incubated overnight at 4 °C with the following primary antibodies: goat polyclonal anti-cIAP1 antibody (R& D Systems, Abingdon, UK), goat polyclonal anti-XIAP antibody (R& D Systems, Abingdon, UK), rabbit polyclonal anti-cleaved PARP (Cell Signaling Technology Inc., Danvers, USA) and rabbit monoclonal anti-cleaved caspase-3 (Cell Signaling Technology Inc., Danvers, USA). After washing and incubation with the appropriate IR-conjugated secondary antibody (LI-COR, Cambridge, UK), detection was achieved using an Odyssey Infrared Imaging System (LI-COR, Cambridge, UK).

Pharmacokinetic studies in MDA-MB-231 Xenografts

Pharmacokinetic studies were performed in male Balb/c severe combined immunodeficient (SCID) mice bearing MDA-MB-231 xenograft tumours in accordance with the Animal (Scientific Procedures) Act (1986) law. A single dose of compound **21** at 100 mg/kg, formulated in 10% DMSO/90% Saline at a dose volume of 10 mL/kg, was administered to 12 mice via intraperitoneal injection. Doses were calculated as freebase equivalent per kg of bodyweight. Following dosing, blood samples (0.2 mL) were drawn in tubes containing potassium EDTA, via either saphenous vein bleeding or cardiac puncture at various time points over 24 hours using sparse sampling (n = 3 per time point), prior to centrifugation (2000 *g* at 4 °C, 10 min). The resultant plasma was separated from the erythrocyte pellets for analysis and stored at -20 °C. Tumours were immediately excised and flash-frozen in liquid nitrogen. Tumour samples were prepared by homogenisation in water (5 mL/g tumour tissue) using a Precellys 24® tissue homogeniser. All samples were extracted by protein precipitation with acetonitrile containing internal standard (1:3 v/v). Calibration standards

and quality controls were prepared in blank matrix and extracted under the same conditions. All samples were centrifuged at 3700 rpm at 4 °C for 20 min. Resultant supernatant was analysed by using high performance liquid chromatography mass spectrometry with either a Quattro Ultima (Waters, UK) tandem mass spectrometer coupled to a CTC HTS PAL autosampler (CTC Analytics AG, Switzerland). Non-compartmental pharmacokinetic (PK) analyses were performed using WinNonLin (Pharsight, Inc.) software. Calculated parameters included time of maximum observed concentration (T_{max}), maximum concentration (C_{max}), terminal half-life, area under the curve (AUC) from the time of dosing to the last measurable concentration (AUC_{last}) and extrapolated to infinity ($AUC_{0-\infty}$). Non-compartmental PK fitting to sparse sampling data allowed the calculation of standard errors on AUC_{last} and C_{max}.

***In Vivo* Efficacy Study**

In order to demonstrate efficacy in a mouse xenograft model, Balb/c scid mice were inoculated sub- cutaneously with 5 x 10^6 MDA-MB-231 cells and xenografts were allowed to reach a group (n=8) average volume of 100 mm^3 before starting the study. 100 mg/kg i.p. doses of **21** were administered b.i.d. in and as a positive control in this study the clinical IAP antagonist, Debio-1143, was dosed daily (q.d.) at 100 mg/kg p.o. compared to a vehicle only control group. Tumor volumes were calculated from tumor size measurements (length x width x width x 0.5) taken every 3 days and the effect on body weight was recorded on a daily basis. For PK/PD studies tumors were excised at specific times post compound dose and snap frozen in liquid nitrogen before being stored at – 80 °C prior to analysis.

Computational Protocols

Docking. Docking experiments were used to predict the binding mode of designed piperazines and to select compounds for synthesis. The X-ray crystal structure of XIAP-BIR3 with compound **1** was used to dock ligands. Hydrogens were added to the protein, and a

binding pocket was generated with all protein atoms within 6 Å of any non-hydrogen atom in ligand **1**. This binding site was used to run dockings and virtual screens for ligands designed to bind to the P1, P2 and P3 pockets. All calculations were run on a Linux cluster using Goldscore[26] scoring function within the Astex Web-based docking and virtual screening platform.[27] Methods and settings have been previously described by Verdonk et al.[28]

***Ab initio* calculations.** The electrostatic potential surfaces of compound **8** and **17** were calculated using the *ab initio* quantum chemistry package Q-Chem,[29] using the 6-31G* basis set and B3LYP method.

Field points. The field points of compound **7** were generated with XEDVIEW, using methods and setting previously described by Cheeseright et al.[21]

ASSOCIATED CONTENT

Supporting Information

Protein production for bioassay, crystallography and NMR. Synthesis of compounds 5, 8-20 and 22-31. This material is available free of charge via the Internet at http://pubs.acs.org.

Accession Codes

Coordinates for XIAP-BIR3 complexes with compounds **1**, **2**, **3**, **4**, **5**, **7**, **17**, **18**, **20** and **21** have been deposited in the Protein Data Bank (PDB) under accession codes 5c3h, 5c0l, 5c0k, 5c3k, 5c7b, 5c7a, 5c7d, 5c7c, 5c84 and 5c83, respectively.

AUTHOR INFORMATION

Corresponding Author

E-mail: gianni.chessari@astx.com. Phone: +44 (0) 1223 226215

ACKNOWLEDGMENTS

We warmly acknowledge scientific discussions with many Astex colleagues including Chris Murray, Tom Heightman, Harren Jhoti and Puja Pathuri.

ABBREVIATIONS USED

cIAP1, cellular inhibitor of apoptosis protein 1; XIAP, X-linked inhibitor of apoptosis protein; BIR, baculovirus IAP repeat domain; RING, really interesting new gene; TNFα, tumor necrosis factor alpha; SMAC, second mitochondria derived activator of caspases; RIPK1, receptor-interacting serine/threonine-protein kinase 1; FADD, Fas-associated protein with Death Domain; FBDD, fragment-based drug discovery; PPI, protein-protein interaction; LE, ligand efficiency; Cbz, carbobenzyloxy; EDC, 1-Ethyl-3-(3-dimethylaminopropyl)carbodiimide; DIPEA, N,N-Diisopropylethylamine; DCM, dichloromethane; THF, tetrahydrofuran; TEA, Triethylamine; SEM, 2-trimethylsilylethyoxymethyl; RT, room temperature;

REFERENCES

1. Hanahan, D.; Weinberg, R. A., Hallmarks of cancer: the next generation. *Cell* **2011,** *144* (5), 646-674.

2. (a) Salvesen, G. S.; Duckett, C. S., IAP proteins: blocking the road to death's door. *Nat. Rev. Mol. Cell Biol.* **2002,** *3* (6), 401-10; (b) Gyrd-Hansen, M.; Meier, P., IAPs: from caspase inhibitors to modulators of NF-kappaB, inflammation and cancer. *Nat. Rev. Cancer* **2010,** *10* (8), 561-74; (c) Silke, J.; Meier, P., Inhibitor of apoptosis (IAP) proteins-modulators of cell death and inflammation. *Cold Spring Harb. Perspect. Biol.* **2013,** *5* (2), 1-19.

3. (a) Tamm, I.; Richter, S.; Oltersdorf, D.; Creutzig, U.; Harbott, J.; Scholz, F.; Karawajew, L.; Ludwig, W. D.; Wuchter, C., High expression levels of X-linked inhibitor of apoptosis protein and survivin correlate with poor overall survival in childhood de novo acute myeloid leukemia. *Clin. Cancer Res.* **2004,** *10* (11), 3737-3744; (b) Mizutani, Y.; Nakanishi,

H.; Li, Y. N.; Matsubara, H.; Yamamoto, K.; Sato, N.; Shiraishi, T.; Nakamura, T.; Mikami, K.; Okihara, K.; Takaha, N.; Ukimura, O.; Kawauchi, A.; Nonomura, N.; Bonavida, B.; Miki, T., Overexpression of XIAP expression in renal cell carcinoma predicts a worse prognosis. *Int. J. Oncol.* **2007,** *30* (4), 919-925; (c) Fulda, S.; Vucic, D., Targeting IAP proteins for therapeutic intervention in cancer. *Nat. Rev. Drug Discov.* **2012,** *11* (2), 109-124.

4. (a) Miller, L. K., An exegesis of IAPs: salvation and surprises from BIR motifs. *Trends Cell Biol.* **1999,** *9* (8), 323-328; (b) Verhagen, A. M.; Coulson, E. J.; Vaux, D. L., Inhibitor of apoptosis proteins and their relatives: IAPs and other BIRPs. *Genome Biol.* **2001,** *2* (7), 1-10; (c) Varfolomeev, E.; Vucic, D., (Un)expected roles of c-IAPs in apoptotic and NFkappaB signaling pathways. *Cell Cycle* **2008,** *7* (11), 1511-1521.

5. (a) Chai, J.; Shiozaki, E.; Srinivasula, S. M.; Wu, Q.; Datta, P.; Alnemri, E. S.; Shi, Y., Structural basis of caspase-7 inhibition by XIAP. *Cell* **2001,** *104* (5), 769-780; (b) Riedl, S. J.; Renatus, M.; Schwarzenbacher, R.; Zhou, Q.; Sun, C.; Fesik, S. W.; Liddington, R. C.; Salvesen, G. S., Structural basis for the inhibition of caspase-3 by XIAP. *Cell* **2001,** *104* (5), 791-800; (c) Shiozaki, E. N.; Chai, J.; Rigotti, D. J.; Riedl, S. J.; Li, P.; Srinivasula, S. M.; Alnemri, E. S.; Fairman, R.; Shi, Y., Mechanism of XIAP-mediated inhibition of caspase-9. *Mol. Cell* **2003,** *11* (2), 519-527; (d) Scott, F. L.; Denault, J. B.; Riedl, S. J.; Shin, H.; Renatus, M.; Salvesen, G. S., XIAP inhibits caspase-3 and -7 using two binding sites: evolutionarily conserved mechanism of IAPs. *EMBO J.* **2005,** *24* (3), 645-655.

6. Behrends, C.; Harper, J. W., Constructing and decoding unconventional ubiquitin chains. *Nat. Struct. Mol. Biol.* **2011,** *18* (5), 520-528.

7. Varfolomeev, E.; Goncharov, T.; Fedorova, A. V.; Dynek, J. N.; Zobel, K.; Deshayes, K.; Fairbrother, W. J.; Vucic, D., c-IAP1 and c-IAP2 are critical mediators of tumor necrosis

factor alpha (TNFalpha)-induced NF-kappaB activation. *J. Biol. Chem.* **2008,** *283* (36), 24295-2499.

8. (a) Liu, Z.; Sun, C.; Olejniczak, E. T.; Meadows, R. P.; Betz, S. F.; Oost, T.; Herrmann, J.; Wu, J. C.; Fesik, S. W., Structural basis for binding of Smac/DIABLO to the XIAP BIR3 domain. *Nature* **2000,** *408* (6815), 1004-1008; (b) Wu, G.; Chai, J.; Suber, T. L.; Wu, J. W.; Du, C.; Wang, X.; Shi, Y., Structural basis of IAP recognition by Smac/DIABLO. *Nature* **2000,** *408* (6815), 1008-1012.

9. (a) Yang, Q. H.; Du, C., Smac/DIABLO selectively reduces the levels of c-IAP1 and c-IAP2 but not that of XIAP and livin in HeLa cells. *J. Biol. Chem.* **2004,** *279* (17), 16963-16970; (b) Phillips, A. H.; Schoeffler, A. J.; Matsui, T.; Weiss, T. M.; Blankenship, J. W.; Zobel, K.; Giannetti, A. M.; Dueber, E. C.; Fairbrother, W. J., Internal motions prime cIAP1 for rapid activation. *Nat. Struct. Mol. Biol.* **2014,** *21* (12), 1068-1074.

10. (a) Petersen, S. L.; Wang, L.; Yalcin-Chin, A.; Li, L.; Peyton, M.; Minna, J.; Harran, P.; Wang, X., Autocrine TNFalpha signaling renders human cancer cells susceptible to Smac-mimetic-induced apoptosis. *Cancer Cell* **2007,** *12* (5), 445-456; (b) Wang, L.; Du, F.; Wang, X., TNF-alpha induces two distinct caspase-8 activation pathways. *Cell* **2008,** *133* (4), 693-703.

11. Ndubaku, C.; Varfolomeev, E.; Wang, L.; Zobel, K.; Lau, K.; Elliott, L. O.; Maurer, B.; Fedorova, A. V.; Dynek, J. N.; Koehler, M.; Hymowitz, S. G.; Tsui, V.; Deshayes, K.; Fairbrother, W. J.; Flygare, J. A.; Vucic, D., Antagonism of c-IAP and XIAP proteins is required for efficient induction of cell death by small-molecule IAP antagonists. *ACS Chem. Biol.* **2009,** *4* (7), 557-566.

12. (a) Sweeney, M. C.; Wang, X.; Park, J.; Liu, Y.; Pei, D., Determination of the sequence specificity of XIAP BIR domains by screening a combinatorial peptide library.

Biochemistry (Mosc.) **2006,** *45* (49), 14740-14748; (b) Seneci, P.; Bianchi, A.; Battaglia, C.; Belvisi, L.; Bolognesi, M.; Caprini, A.; Cossu, F.; Franco, E.; Matteo, M.; Delia, D.; Drago, C.; Khaled, A.; Lecis, D.; Manzoni, L.; Marizzoni, M.; Mastrangelo, E.; Milani, M.; Motto, I.; Moroni, E.; Potenza, D.; Rizzo, V.; Servida, F.; Turlizzi, E.; Varrone, M.; Vasile, F.; Scolastico, C., Rational design, synthesis and characterization of potent, non-peptidic Smac mimics/XIAP inhibitors as proapoptotic agents for cancer therapy. *Bioorg. Med. Chem.* **2009,** *17* (16), 5834-5856; (c) Sharma, S. K.; Straub, C.; Zawel, L., Development of Peptidomimetics Targeting IAPs. *International journal of peptide research and therapeutics* **2006,** *12* (1), 21-32; (d) Kester, R. F.; Donnell, A. F.; Lou, Y.; Remiszewski, S. W.; Lombardo, L. J.; Chen, S.; Le, N. T.; Lo, J.; Moliterni, J. A.; Han, X.; Hogg, J. H.; Liang, W.; Michoud, C.; Rupert, K. C.; Mischke, S.; Le, K.; Weisel, M.; Janson, C. A.; Lukacs, C. M.; Fretland, A. J.; Hong, K.; Polonskaia, A.; Gao, L.; Li, S.; Solis, D. S.; Aguilar, D.; Tardell, C.; Dvorozniak, M.; Tannu, S.; Lee, E. C.; Schutt, A. D.; Goggin, B., Optimization of benzodiazepinones as selective inhibitors of the X-linked inhibitor of apoptosis protein (XIAP) second baculovirus IAP repeat (BIR2) domain. *J. Med. Chem.* **2013,** *56* (20), 7788-7803; (e) Oost, T. K.; Sun, C.; Armstrong, R. C.; Al-Assaad, A. S.; Betz, S. F.; Deckwerth, T. L.; Ding, H.; Elmore, S. W.; Meadows, R. P.; Olejniczak, E. T.; Oleksijew, A.; Oltersdorf, T.; Rosenberg, S. H.; Shoemaker, A. R.; Tomaselli, K. J.; Zou, H.; Fesik, S. W., Discovery of potent antagonists of the antiapoptotic protein XIAP for the treatment of cancer. *J. Med. Chem.* **2004,** *47* (18), 4417-4426.

13. (a) Wong, H.; Gould, S. E.; Budha, N.; Darbonne, W. C.; Kadel, E. E., 3rd; La, H.; Alicke, B.; Halladay, J. S.; Erickson, R.; Portera, C.; Tolcher, A. W.; Infante, J. R.; Mamounas, M.; Flygare, J. A.; Hop, C. E.; Fairbrother, W. J., Learning and confirming with preclinical studies: modeling and simulation in the discovery of GDC-0917, an inhibitor of apoptosis proteins antagonist. *Drug Metab. Dispos.* **2013,** *41* (12), 2104-2113; (b) Dhuria, S.;

Einolf, H.; Mangold, J.; Sen, S.; Gu, H.; Wang, L.; Cameron, S., Time-dependent inhibition and induction of human cytochrome P4503A4/5 by an oral IAP antagonist, LCL161, in vitro and in vivo in healthy subjects. *J. Clin. Pharmacol.* **2013,** *53* (6), 642-653; (c) Cai, Q.; Sun, H.; Peng, Y.; Lu, J.; Nikolovska-Coleska, Z.; McEachern, D.; Liu, L.; Qiu, S.; Yang, C. Y.; Miller, R.; Yi, H.; Zhang, T.; Sun, D.; Kang, S.; Guo, M.; Leopold, L.; Yang, D.; Wang, S., A potent and orally active antagonist (SM-406/AT-406) of multiple inhibitor of apoptosis proteins (IAPs) in clinical development for cancer treatment. *J. Med. Chem.* **2011,** *54* (8), 2714-2726; (d) Condon, S. M.; Mitsuuchi, Y.; Deng, Y.; LaPorte, M. G.; Rippin, S. R.; Haimowitz, T.; Alexander, M. D.; Kumar, P. T.; Hendi, M. S.; Lee, Y. H.; Benetatos, C. A.; Yu, G.; Kapoor, G. S.; Neiman, E.; Seipel, M. E.; Burns, J. M.; Graham, M. A.; McKinlay, M. A.; Li, X.; Wang, J.; Shi, Y.; Feltham, R.; Bettjeman, B.; Cumming, M. H.; Vince, J. E.; Khan, N.; Silke, J.; Day, C. L.; Chunduru, S. K., Birinapant, a smac-mimetic with improved tolerability for the treatment of solid tumors and hematological malignancies. *J. Med. Chem.* **2014,** *57* (9), 3666-3677; (e) Flygare, J. A.; Beresini, M.; Budha, N.; Chan, H.; Chan, I. T.; Cheeti, S.; Cohen, F.; Deshayes, K.; Doerner, K.; Eckhardt, S. G.; Elliott, L. O.; Feng, B.; Franklin, M. C.; Reisner, S. F.; Gazzard, L.; Halladay, J.; Hymowitz, S. G.; La, H.; LoRusso, P.; Maurer, B.; Murray, L.; Plise, E.; Quan, C.; Stephan, J. P.; Young, S. G.; Tom, J.; Tsui, V.; Um, J.; Varfolomeev, E.; Vucic, D.; Wagner, A. J.; Wallweber, H. J.; Wang, L.; Ware, J.; Wen, Z.; Wong, H.; Wong, J. M.; Wong, M.; Wong, S.; Yu, R.; Zobel, K.; Fairbrother, W. J., Discovery of a potent small-molecule antagonist of inhibitor of apoptosis (IAP) proteins and clinical candidate for the treatment of cancer (GDC-0152). *J. Med. Chem.* **2012,** *55* (9), 4101-4113; (f) Hashimoto, K.; Saito, B.; Miyamoto, N.; Oguro, Y.; Tomita, D.; Shiokawa, Z.; Asano, M.; Kakei, H.; Taya, N.; Kawasaki, M.; Sumi, H.; Yabuki, M.; Iwai, K.; Yoshida, S.; Yoshimatsu, M.; Aoyama, K.; Kosugi, Y.; Kojima, T.; Morishita, N.; Dougan, D. R.; Snell, G. P.; Imamura, S.; Ishikawa, T., Design and synthesis of potent inhibitor of apoptosis (IAP)

proteins antagonists bearing an octahydropyrrolo[1,2-a]pyrazine scaffold as a novel proline mimetic. *J. Med. Chem.* **2013,** *56* (3), 1228-1246; (g) Hennessy, E. J.; Adam, A.; Aquila, B. M.; Castriotta, L. M.; Cook, D.; Hattersley, M.; Hird, A. W.; Huntington, C.; Kamhi, V. M.; Laing, N. M.; Li, D.; MacIntyre, T.; Omer, C. A.; Oza, V.; Patterson, T.; Repik, G.; Rooney, M. T.; Saeh, J. C.; Sha, L.; Vasbinder, M. M.; Wang, H.; Whitston, D., Discovery of a novel class of dimeric Smac mimetics as potent IAP antagonists resulting in a clinical candidate for the treatment of cancer (AZD5582). *J. Med. Chem.* **2013,** *56* (24), 9897-9919.

14. (a) Scott, D. E.; Coyne, A. G.; Hudson, S. A.; Abell, C., Fragment-based approaches in drug discovery and chemical biology. *Biochemistry (Mosc.)* **2012,** *51* (25), 4990-5003; (b) Murray, C. W.; Rees, D. C., The rise of fragment-based drug discovery. *Nat. Chem.* **2009,** *1* (3), 187-192.

15. (a) Maurer, T.; Wang, W., NMR study to identify a ligand-binding pocket in Ras. *The Enzymes* **2013,** *33 Pt A*, 15-39; (b) Oltersdorf, T.; Elmore, S. W.; Shoemaker, A. R.; Armstrong, R. C.; Augeri, D. J.; Belli, B. A.; Bruncko, M.; Deckwerth, T. L.; Dinges, J.; Hajduk, P. J.; Joseph, M. K.; Kitada, S.; Korsmeyer, S. J.; Kunzer, A. R.; Letai, A.; Li, C.; Mitten, M. J.; Nettesheim, D. G.; Ng, S.; Nimmer, P. M.; O'Connor, J. M.; Oleksijew, A.; Petros, A. M.; Reed, J. C.; Shen, W.; Tahir, S. K.; Thompson, C. B.; Tomaselli, K. J.; Wang, B.; Wendt, M. D.; Zhang, H.; Fesik, S. W.; Rosenberg, S. H., An inhibitor of Bcl-2 family proteins induces regression of solid tumours. *Nature* **2005,** *435* (7042), 677-681; (c) Saalau-Bethell, S. M.; Woodhead, A. J.; Chessari, G.; Carr, M. G.; Coyle, J.; Graham, B.; Hiscock, S. D.; Murray, C. W.; Pathuri, P.; Rich, S. J.; Richardson, C. J.; Williams, P. A.; Jhoti, H., Discovery of an allosteric mechanism for the regulation of HCV NS3 protein function. *Nat. Chem. Biol.* **2012,** *8* (11), 920-925; (d) Scott, D. E.; Ehebauer, M. T.; Pukala, T.; Marsh, M.; Blundell, T. L.; Venkitaraman, A. R.; Abell, C.; Hyvonen, M., Using a fragment-based approach to target protein-protein interactions. *Chembiochem* **2013,** *14* (3), 332-342.

16. Hartshorn, M. J.; Murray, C. W.; Cleasby, A.; Frederickson, M.; Tickle, I. J.; Jhoti, H., Fragment-based lead discovery using X-ray crystallography. *J. Med. Chem.* **2005,** *48* (2), 403-413.

17. Hopkins, A. L.; Groom, C. R.; Alex, A., Ligand efficiency: a useful metric for lead selection. *Drug Discov. Today* **2004,** *9* (10), 430-431.

18. Moore, C. D.; Wu, H.; Bolanos, B.; Bergqvist, S.; Brooun, A.; Pauly, T.; Nowlin, D., Structural and biophysical characterization of XIAP BIR3 G306E mutant: insights in protein dynamics and application for fragment-based drug design. *Chem. Biol. Drug Des.* **2009,** *74* (3), 212-223.

19. Park, C. M.; Sun, C.; Olejniczak, E. T.; Wilson, A. E.; Meadows, R. P.; Betz, S. F.; Elmore, S. W.; Fesik, S. W., Non-peptidic small molecule inhibitors of XIAP. *Bioorg. Med. Chem. Lett.* **2005,** *15* (3), 771-775.

20. Vinter, J. G., Extended electron distributions applied to the molecular mechanics of some intermolecular interactions. *J. Comput. Aided Mol. Des.* **1994,** *8* (6), 653-668.

21. Cheeseright, T.; Mackey, M.; Rose, S.; Vinter, A., Molecular field extrema as descriptors of biological activity: definition and validation. *J. Chem. Inf. Model.* **2006,** *46* (2), 665-676.

22. Cockroft, S. L.; Hunter, C. A.; Lawson, K. R.; Perkins, J.; Urch, C. J., Electrostatic control of aromatic stacking interactions. *J. Am. Chem. Soc.* **2005,** *127* (24), 8594-8595.

23. Mortenson, P. N.; Murray, C. W., Assessing the lipophilicity of fragments and early hits. *J. Comput. Aided Mol. Des.* **2011,** *25* (7), 663-667.

24. Verdonk, M. L.; Rees, D. C., Group efficiency: a guideline for hits-to-leads chemistry. *Chemmedchem* **2008,** *3* (8), 1179-1180.

25. Nociari, M. M.; Shalev, A.; Benias, P.; Russo, C., A novel one-step, highly sensitive fluorometric assay to evaluate cell-mediated cytotoxicity. *J. Immunol. Methods* **1998,** *213* (2), 157-167.

26. Jones, G.; Willett, P.; Glen, R. C., Molecular recognition of receptor sites using a genetic algorithm with a description of desolvation. *J. Mol. Biol.* **1995,** *245* (1), 43-53.

27. Watson, P.; Verdonk, M.; Hartshorn, M. J., A web-based platform for virtual screening. *J. Mol. Graph. Model.* **2003,** *22* (1), 71-82.

28. Verdonk, M. L.; Cole, J. C.; Hartshorn, M. J.; Murray, C. W.; Taylor, R. D., Improved protein-ligand docking using GOLD. *Proteins* **2003,** *52* (4), 609-623.

29. Shao, Y.; Molnar, L. F.; Jung, Y.; Kussmann, J.; Ochsenfeld, C.; Brown, S. T.; Gilbert, A. T.; Slipchenko, L. V.; Levchenko, S. V.; O'Neill, D. P.; DiStasio, R. A., Jr.; Lochan, R. C.; Wang, T.; Beran, G. J.; Besley, N. A.; Herbert, J. M.; Lin, C. Y.; Van Voorhis, T.; Chien, S. H.; Sodt, A.; Steele, R. P.; Rassolov, V. A.; Maslen, P. E.; Korambath, P. P.; Adamson, R. D.; Austin, B.; Baker, J.; Byrd, E. F.; Dachsel, H.; Doerksen, R. J.; Dreuw, A.; Dunietz, B. D.; Dutoi, A. D.; Furlani, T. R.; Gwaltney, S. R.; Heyden, A.; Hirata, S.; Hsu, C. P.; Kedziora, G.; Khalliulin, R. Z.; Klunzinger, P.; Lee, A. M.; Lee, M. S.; Liang, W.; Lotan, I.; Nair, N.; Peters, B.; Proynov, E. I.; Pieniazek, P. A.; Rhee, Y. M.; Ritchie, J.; Rosta, E.; Sherrill, C. D.; Simmonett, A. C.; Subotnik, J. E.; Woodcock, H. L., 3rd; Zhang, W.; Bell, A. T.; Chakraborty, A. K.; Chipman, D. M.; Keil, F. J.; Warshel, A.; Hehre, W. J.; Schaefer, H. F., 3rd; Kong, J.; Krylov, A. I.; Gill, P. M.; Head-Gordon, M., Advances in methods and algorithms in a modern quantum chemistry program package. *Phys. Chem. Chem. Phys.* **2006,** *8* (27), 3172-3191.

TABLE OF CONTENTS GRAPHIC